

KfK 3516

Juli 1983

# Neutron Capture in s-Wave Resonances of $^{56}\text{Fe}$ , $^{58}\text{Ni}$ , and $^{60}\text{Ni}$

K. Wisshak, F. Käppeler, G. Reffo, and F. Fabbri  
Institut für Angewandte Kernphysik

Kernforschungszentrum Karlsruhe



KERNFORSCHUNGSZENTRUM KARLSRUHE  
Institut für Angewandte Kernphysik

KfK 3516

NEUTRON CAPTURE IN s-WAVE RESONANCES  
OF  $^{56}\text{Fe}$ ,  $^{58}\text{Ni}$ , and  $^{60}\text{Ni}$

K. Wisshak, F. Käppeler, G. Reffo<sup>+</sup>, and F. Fabbri<sup>+</sup>

Kernforschungszentrum Karlsruhe GmbH, Karlsruhe

<sup>+</sup> E.N.E.A. Bologna

Als Manuskript vervielfältigt  
Für diesen Bericht behalten wir uns alle Rechte vor

Kernforschungszentrum Karlsruhe GmbH  
ISSN 0303-4003

## ABSTRACT

The neutron capture widths of s-wave resonances in  $^{56}\text{Fe}$  (27.7 keV),  $^{58}\text{Ni}$  (15.4 keV) and  $^{60}\text{Ni}$  (12.5 keV) have been determined using a setup completely different from previous experiments. A pulsed 3-MV Van de Graaff accelerator and a kinematically collimated neutron beam, produced via the  $^7\text{Li}(p,n)$  reaction, was used in the experiments. Capture gamma-rays were observed by three Moxon-Rae detectors with graphite-, bismuth-graphite-, and bismuth-converters, respectively. The samples were positioned at a neutron flight path of only 8 cm. Thus events due to capture of resonance scattered neutrons in the detectors or in surrounding materials are completely discriminated by their additional time of flight. The high neutron flux at the sample position allowed the use of very thin samples (0.15 mm - 0.45 mm), avoiding large multiple scattering corrections. The data obtained with the individual detectors were corrected for the efficiency of the respective converter materials. For that purpose, detailed theoretical calculations of the capture gamma-ray spectra of the measured isotopes and of gold, which was used as a standard, were performed. The final results are:  $\Gamma_\gamma$  (27.7 keV,  $^{56}\text{Fe}$ ) =  $1.06 \pm 0.05$  eV,  $\Gamma_\gamma$  (15.4 keV,  $^{58}\text{Ni}$ ) =  $1.53 \pm 0.10$  eV and  $\Gamma_\gamma$  (12.5 keV,  $^{60}\text{Ni}$ ) =  $2.92 \pm 0.19$  eV. The accuracy obtained with the present experimental method represents an improvement of a factor 3-6 compared to previous experiments. The investigated s-wave resonances contribute 10 - 40 % to the total capture rate of the respective isotopes in a typical fast reactor.

## ZUSAMMENFASSUNG

Neutroneneinfang in s-Wellen Resonanzen von  $^{56}\text{Fe}$ ,  $^{58}\text{Ni}$  und  $^{60}\text{Ni}$

Die Neutroneneinfangbreite von s-Wellen Resonanzen in  $^{56}\text{Fe}$  (27.7 keV),  $^{58}\text{Ni}$  (15.4 keV) und  $^{60}\text{Ni}$  (12.5 keV) wurde mit einem Versuchsaufbau gemessen, der sich völlig von denen früherer Messungen unterscheidet. Mit einem gepulsten 3 MV Van de Graaff Beschleuniger wurde ein kinematisch kollimierter Neutronenstrahl über die  $^7\text{Li}(p,n)$  Reaktion erzeugt. Die Gammaquanten des Neutroneneinfangs wurden mit drei verschiedenen Moxon-Rae-Detektoren gemessen, die mit einem Graphit-, Wismut-Graphit- bzw. einem Wismut-Konverter ausgerüstet waren. Die Proben waren unter einem Flugweg von nur 8 cm aufgestellt. Auf diese Weise wurden Ereignisse, die durch Einfang gestreuter Neutronen im Detektor oder dem umgebenden Material verursacht werden, vollständig über die zusätzliche Flugzeit diskriminiert. Der hohe Neutronenfluß am Ort der Probe erlaubte die Verwendung von sehr dünnen Proben (0.15 - 0.45 mm). Auf diese Weise wurden große Vielfachstreuorkorrekturen vermieden. Die mit den verschiedenen Detektoren gemessenen Daten wurden auf die unterschiedliche Ansprechwahrscheinlichkeit der einzelnen Konvertermaterialien korrigiert. Dazu wurden umfangreiche theoretische Rechnungen durchgeführt, um die Einfang-Gammaspektren der einzelnen Isotope und des Gold-Standards zu bestimmen. Die Ergebnisse sind:  $\Gamma_\gamma$  (27.7 keV,  $^{56}\text{Fe}$ ) =  $1.06 \pm 0.05$  eV,  $\Gamma_\gamma$  (15.4 keV,  $^{58}\text{Ni}$ ) =  $1.53 \pm 0.10$  eV und  $\Gamma_\gamma$  (12.5 keV,  $^{60}\text{Ni}$ ) =  $2.92 \pm 0.19$  eV. Die Genauigkeit der verwendeten experimentellen Methode ist um einen Faktor 3-6 besser als die früherer Messungen. Die untersuchten Resonanzen tragen 10 - 40 % zur totalen Einfangrate des jeweiligen Isotopes in einem typischen schnellen Reaktor bei.

## I. INTRODUCTION

The exact determination of the capture widths of broad s-wave resonances in structural materials is an important problem in fast reactor physics because of two reasons: (i) By their large capture area, these resonances contribute significantly to the capture cross section averaged over the reactor spectrum.

(ii) In previous measurements their large ratio  $\Gamma_n/\Gamma_\gamma \sim 10^3$  caused severe systematic uncertainties due to capture of resonance scattered neutrons. These difficulties are strikingly illustrated at the example of  $\Gamma_\gamma$  for the 27.7 keV resonance in  $^{56}\text{Fe}$  where the published values vary by a factor of two<sup>1</sup>.

Recently, a careful reevaluation of the Oak Ridge data<sup>2,3</sup> for  $^{58,60}\text{Ni}$  showed that the present accuracy for strong s-wave resonances around  $\sim 10$  keV is limited to  $\sim 30\%$ . These uncertainties do not meet the requests formulated for capture cross sections of structural materials<sup>4</sup>.

Part of the experimental difficulties have been overcome in LINAC experiments by the use of arrangements with very low neutron sensitivity<sup>5,6</sup>. In the present work, which was performed at a Van de Graaff accelerator, a completely different approach was made to solve the problems. Events due to capture of resonance scattered neutrons are discriminated completely by time-of-flight (TOF). This was possible using an experimental setup where the primary flight path of the neutrons is shorter than the distance from sample to detector. This approach has the additional advantage of a very high neutron flux at the sample position thus allowing for thinner samples than were used in any other capture measurement. In this way sample related uncertainties were greatly reduced, e.g. due to large multiple scattering corrections.

The experimental method has been described already in Ref. 1, where the capture width of the 27.7 keV resonance in  $^{56}\text{Fe}$  was determined. In this first measurement a Moxon-Rae detector with graphite converter was used to registrate the capture gamma-rays.

The largest systematic uncertainty was due to deviations of the detector efficiency from the ideal shape (which is linearly increasing with gamma-ray energy). To reduce this problem in the present experiment, data were taken simultaneously with three Moxon-Rae detectors which were equipped with graphite, bismuth-graphite and bismuth converters, respectively. The capture width as determined with each of the three detectors was corrected for the efficiency of the respective converter. For this purpose detailed theoretical calculations were performed in the framework of the statistical and spherical optical model to determine the shape of the capture gamma-ray spectra for the investigated isotopes and for gold, which was used as a standard. These spectra together with the shape of the detector efficiencies (evaluated from literature) allowed for a correction of the results which were obtained with the individual detectors. The final values for  $\Gamma_\gamma$  agreed within the remaining total systematic uncertainty of 5 - 6 %.

With this modified setup the measurements on  $^{56}\text{Fe}$  were repeated and extended to the s-wave resonances at 15.4 and 12.5 keV in  $^{58}\text{Ni}$  and  $^{60}\text{Ni}$ , respectively. In case of  $^{56}\text{Fe}$ , data were taken from two samples (0.3 mm and 2.0 mm thickness) while for each nickel isotope three samples were used (0.15, 0.3 and 0.45 mm). It has to be noted that the 0.15 mm sample is nearly a factor of three thinner than the thinnest sample used up to now. The final data have a total uncertainty of 5 - 7 % thus satisfying the current requests <sup>4</sup>.

## II. EXPERIMENTS

The experiment is an optimized version of a setup proposed by Macklin et al. <sup>7</sup> already in 1963. A schematic drawing is shown in Fig. 1. The measurements were performed at the Karlsruhe 3-MV pulsed Van de Graaff accelerator. A kinematically collimated neutron beam is produced via the  $^7\text{Li}(p,n)$  reaction by adjusting the proton energy just above the reaction threshold.

In this case no further collimation is required and the samples can be placed at a flight path as short as 9 cm. The capture detectors are arranged at backward angles completely outside the neutron cone. The distance from sample to detector is  $\sim 16$  cm. Data were taken simultaneously from three Moxon-Rae detectors with graphite, bismuth-graphite and pure bismuth converters, respectively. Two  ${}^6\text{Li}$ -glass detectors are used to ensure that all samples are irradiated by the same neutron fluence. A TOF-spectrum is recorded from a transmission detector located at  $0^\circ$  with respect to the beam axis and a pulse height spectrum is taken from a neutron monitor at  $20^\circ$ .

Five samples are used in each run: two isotopes of the structural materials under investigation, a gold sample as a cross section standard, a graphite sample as a pure scatterer and an empty position in the sample changer frame for background determination. Details of the experimental methods, data evaluation and systematic uncertainties are given in Ref. 1. The important parameters of the individual samples are compiled in Table I.

The main advantages of this setup are the following:

- 1.) The distance between samples and detectors is a factor of two larger than the flight path of the primary neutrons. Thus, events due to capture of scattered neutrons in the detector or in surrounding materials are completely discriminated by the additional TOF.
- 2.) The high neutron flux at the sample position allowed the use of very thin samples (e.g., 0.15 mm for  ${}^{58,60}\text{Ni}$ , the isotopes of main interest).
- 3.) The limited energy range of the neutron spectrum from 10 to 60 keV avoids unwanted background from scattering resonances at higher energies.
- 4.) The total time resolution of 1.2 ns is sufficient to separate the s-waves from neighbouring p-wave resonances (except for  ${}^{60}\text{Ni}$ ).

Due to the high binding energy of  $^{58}\text{Ni}$  (9 MeV) the thickness of the converters was adjusted to stop electrons up to 10 MeV energy. At that energy the range of electrons is 5.64 g/cm<sup>2</sup> in graphite and 6.0 g/cm<sup>2</sup> in bismuth according to Ref. 8. The actual converter thickness was 34 mm (5.6 g/cm<sup>2</sup>) for graphite and 7 mm (6.8 g/cm<sup>2</sup>) for bismuth. The bismuth-graphite converter was kindly ceded to us by R.L. Macklin and corresponds to the specifications given in Ref. 7.

In order to study the individual systematic uncertainties in detail several runs were made with modified experimental conditions. This is possible only, because the high neutron flux at the sample position reduces significantly the measuring time compared to previous experiments.

The proton energy was adjusted at three different energies (20 keV, 13 keV and 6 keV) above the reaction threshold of the  $^7\text{Li}(p,n)$  reaction. In this way continuous neutron spectra in the energy range 5 to 90 keV, 7 to 75 keV and 10 to 60 keV were obtained, respectively. The neutron flux integrated over the total spectrum scales approximately as 2.5:1.7:1 while ratios of 1.5:1.2:1 are found for the flux at the energy of the s-wave resonances. An essential part of the background being correlated with the total neutron flux, a better statistical accuracy is obtained at high proton energies but at the expense of a lower signal to background ratio compared to the measurements at lower proton energies.

For each nickel isotope three samples were used with thicknesses between 0.15 and 0.45 mm. In the seventh column of Table I the correction for multiple scattering in the investigated s-wave resonance as calculated with the FANAC code (see Section III) is shown to vary for these cases by a factor of three. For  $^{56}\text{Fe}$ , measurements with three different sample thicknesses between 0.15 and 0.6 mm were published already in Ref. 1 so that we could restrict ourselves in this work to one sample of 0.3 mm thickness. But as an additional check a 2 mm thick sample was used, to demonstrate that the multiple scattering correction of the present analysis

works correctly even in such extreme cases. This point was mainly motivated by the experiment of Allen et al.<sup>9</sup> where a similar technique was used but where a discrepant result was obtained with a sample of 2.4 mm thickness.

The important parameters of the individual Runs are compiled in Table II. It should be noted that - except for the thinnest samples - a measuring time of less than one day per sample was sufficient. To demonstrate the effect-to-background ratio Fig. 2 shows the measured TOF spectra of Run II (0.3 mm sample thickness) for all three detectors. As no significant difference is found for the individual converter materials only the spectra measured with the graphite converter are plotted in Fig. 3 for Runs I, III, and IV. The respective spectra of the  $^{56}\text{Fe}$  sample are given in Fig. 4. Comparison of the spectra of Run I and IV in Fig. 3 immediately demonstrates that the signal to background ratio is increasing with decreasing proton energy but at the expense of statistical accuracy. Both runs were taken with the same sample and about the same measuring time but at proton energies 20 keV and 6 keV above the threshold, respectively (see Table II).

### III. DATA ANALYSIS

#### III A Evaluation of the Capture Yield

The data analysis has been described in detail in Ref. 1. Therefore it is here sufficient to point out where changes in the evaluation were made and to discuss the individual correction factors. For all Runs the spectra of the three Moxon-Rae detectors were analyzed separately.

##### 1.) Correction for Electronic Drifts.

The shift of the position of the prompt gamma-ray peak as observed in the individual measurements during one day was always less than one channel (360 ps). Therefore no correction was applied for this effect.

2.) Transformation to a Common Flight Path.

The flight path varied by  $\pm 0.7$  mm for different neutron targets and by  $\pm 0.3$  mm for different samples. This effect was corrected as described in Ref. 1.

3.) Normalization to Equal Neutron Fluence per Sample.

The correction factors for normalization of the TOF spectra to equal neutron fluence which were determined from the data measured with the two  $^6\text{Li}$ -glass monitors were always less than 1.1 %. This holds expect for Run III and for the measurement with the 2.0 mm thick iron sample. In these cases corrections up to 4 % and 2.1 % had to be applied, respectively, which were caused by a temporary instability of the accelerator during Run III and by the short measuring time for the thick iron sample (see Table II).

4.) Subtraction of Time-Dependent Background.

An additional normalization of the background measured with the graphite sample and the empty position as discussed in Ref. 1 was not necessary. In the present experiment the gamma intensity (given by the integrated count rate of the prompt gamma-ray peak) and the neutron beam intensity (detemined as described above) agreed on the average to better than 0.4 %. The only exceptions are again Run III and the spectra for the thick iron sample. In the present evaluation the background spectra were used without smoothing.

5.) Subtraction of a Constant Background.

After subtraction of the time-dependent background (see above) an additional time-independent background was observed. This can be explained by capture of neutrons scattered in the strong s-wave resonances. These events are spread out in time and appear therefore as a constant background in the 50 ns wide time window, which is actually used in the measurement. It is obvious that this background cannot be accounted for by the spectra measured with the graphite sample or without sample. It was determined in three time windows, one on the left hand side and two on the right hand side of the prompt gamma-ray peak. This constant background was always less than 2 % of the background measured without sample.

It has to be noted that in this way a possible uncertainty is accounted for which might be due to the fact that we did not normalize the time-dependent background. The background under the resonance differs only by  $\sim 30\%$  from the background on the right hand side of the gamma-ray peak. Therefore the difference between subtracting a constant background instead of a  $0.4\%$  higher or lower time dependent background is small compared to the uncertainty quoted for the constant background.

6.) Correction for Multiple Scattering and Self-Shielding in the Gold Sample.

In the present experiment the same gold sample was used as in Ref. 1. Therefore the correction factor quoted in Table I is the same.

7.) Correction for Gamma-Ray Self-Absorption.

The correction factors SA for gamma-ray self absorption in the samples calculated according to Ref. 1 are compiled in Table I. The capture yield has to be corrected by a factor  $SA(\text{gold}) / SA(\text{isotope})$ . This factor is always less than  $1\%$  except for the thick iron sample where it amounts to  $2\%$ . Therefore only the capture yield measured with this sample was corrected.

Further support for the method to calculate SA comes from a measurement of the self-absorption using gold samples of different thickness. There,  $SA = 0.987$  was found for a  $0.25\text{ mm}$  thick sample, in excellent agreement with the calculated correction.

8.) Gold Standard Cross Section.

In the present evaluation we used the ENDF/B-V cross section for gold to convert the experimental ratios to absolute values. In order to achieve a compatible energy resolution, we interpolated the ENDF/B-data for each TOF channel and smoothed them according to the width of the prompt gamma-ray peak ( $\text{FWHM} \sim 4$  channels)

It has to be noted that the results of the experimental capture cross sections of Macklin et al. <sup>10</sup> have been revised recently <sup>11</sup> by  $-3.3\%$  at  $10\text{ keV}$  and  $-1\%$  at  $30\text{ keV}$ . The ENDF/B-V evaluation being mainly based on this experiment, this might also have implications for our data.

### III B Determination of the Capture Widths.

To determine the capture widths of s-wave resonances the capture yield was analyzed with the FANAC code of Fröhner<sup>12</sup>. The analysis was performed in the same way as described in Ref. 1. Most of the samples were highly enriched (> 99 %) and therefore isotopic impurities were considered only for the natural iron sample of 2 mm thickness. Parameters used as fixed input for the analysis are compiled in Table III. These values are mainly taken from the work of Fröhner<sup>13,14</sup>. The g values and  $\Gamma_n$  of p-wave resonances were arbitrarily assigned as only  $g\Gamma_n\Gamma_\gamma/\Gamma$  is varied as a free parameter in the fits but it was ensured that  $\Gamma_n \gg \Gamma_\gamma$  since otherwise the sensitivity of the fits to  $\Gamma_\gamma$  is strongly reduced.

In case of the nickel isotopes the analysis was complicated as the s-wave resonances are superposed by p-wave resonances. In <sup>58</sup>Ni the two p-wave resonances at 13.4 and 13.6 keV are resolved from the s-wave resonance at 15.4 keV and thus both components can be separated in the fit. In <sup>60</sup>Ni the two weak p-wave resonances at 12.2 and 13.6 keV are completely hidden in the area of the 12.5 keV s-wave resonance. In order to get a reliable separation of s- and p- components the analysis was performed in two ways:

a.)  $\Gamma_n$  and  $\Gamma_\gamma$  of the s-wave resonance were taken as free parameters. Because of the very short flight path the shape of the resonance is strongly influenced by the time resolution. The full width at half maximum of the prompt gamma-ray peak was taken as a first guess of the time resolution but it turned out that scattering of gamma-rays in the target backing or in the lead shielding around the target increased the width of the gamma peak over the genuine time resolution of the experiment. Therefore, the value for the time resolution, which is used as input in the code was slightly reduced in order to fit the p-wave resonances. This procedure, however, is relatively uncertain as no well isolated p-wave resonance is observed in the spectra with good statistics. The doublet at  $\sim 23.9$  keV in <sup>60</sup>Ni is the best candidate for this adjustment. As an alternative we therefore

decided to treat the s-wave neutron width  $\Gamma_n$  as a free parameter thus accounting properly for the uncertainty in the time resolution. However, one has to be aware that this procedure tends to increase  $\Gamma_n$  also by inclusion of part of the area of overlapping p-wave resonances. This was most pronounced for the p-wave resonances close to the 15.35 keV resonance in  $^{58}\text{Ni}$ .

b.)  $\Gamma_n$  was taken as a fixed parameter using values from Ref.15. In order to check for consistency and to study the effect of p-wave contributions the unresolved multiplets of p-wave resonances at higher energies were analysed, too. Figs. 5 to 9 show the final FANAC fits of the capture yield as evaluated from the spectra shown in Figs. 2 to 4.

### III C      Correction for Detector Efficiency

-----

The main systematic uncertainty in our measurements on structural material isotopes relative to a gold standard is caused by the efficiency of the Moxon-Rae detectors. It deviates from the ideal shape, which is linearly increasing with gamma-ray energy. Neutron capture in structural materials is characterized by a low multiplicity of the associated gamma-ray cascades. Consequently, the capture gamma-ray spectrum is dominated by a hard component caused by transitions to the ground state or the first excited levels and by a soft component from the ground state decay of these low lying states. On the other hand, the high level density in gold yields a higher multiplicity of the cascades and thus a softer spectrum. This difference leads to a systematic uncertainty in the measured cross section ratio. In case of  $^{56}\text{Fe}$  the binding energy of sample and reference sample differ only by  $\sim 20\%$  and the uncertainty may be tolerable. For the nickel isotopes this difference increases up to  $40\%$  and thus reliable data can be obtained only by proper correction for this effect.

In the present experiment data were taken with three different converter materials and the correction was applied for each detector separately. In this way we tried to overcome the un-

certainty which is caused by the fact that the efficiency of the individual converter materials is not known with good accuracy. At least, the remaining differences in the results after correction allow to estimate the systematic uncertainty of this effect.

The evaluation of the efficiency correction, which had (to a lesser extent) also affected our measurements on actinide isotopes, is described in detail in Ref. 16. Two pieces of information are required: the relative shape of the detector efficiency  $\epsilon(E_\gamma)$  and the relative shape of the capture gamma-ray spectrum  $I(E_\gamma)$ . From these data, an effective efficiency,  $\bar{\epsilon}$ , is calculated for each isotope and converter material according to the relation:

$$\bar{\epsilon} = \frac{\int \epsilon(E_\gamma) I(E_\gamma) dE_\gamma}{\int \tilde{\epsilon}(E_\gamma) I(E_\gamma) dE_\gamma}$$

where  $\tilde{\epsilon}(E_\gamma) = C \cdot E_\gamma$  is the ideal shape of the detector efficiency.

The final correction factor  $K_{i,Au}$  with which the values for the resonance parameters have to be multiplied is given by

$$K_{i,Au} = \frac{\bar{\epsilon}_{Au}}{\bar{\epsilon}_i}$$

This correction factor depends not only on the converter material and on the measured isotope  $i$ , but in addition also on spin and parity of the resonance considered, as the capture gamma-ray spectrum is affected by these quantum numbers via selection rules for electromagnetic transitions.

Two possible shapes for the efficiency of the graphite converter were used, one as evaluated from experimental data in Ref. 1 and the other as calculated by Malik and Majkrzak<sup>17</sup>. The efficiency of the bismuth-graphite detector was taken from Ref. 7. For the bismuth converter we used the average of the calculation in Ref. 17 and the Monte Carlo simulation by Iyengar et al.<sup>18</sup>. The various efficiency curves are shown in Fig. 10.

The capture gamma-ray spectra were calculated in the framework of the statistical model and the spherical optical model. The method is described in Ref. 19 where the results for gold are already published. Details of the calculations for the structural materials are given in Sec. VII. These calculations have been performed for s-, p- and d-wave resonances and for all possible spin values, separately. As for the narrow p- and d-wave resonances in many cases the spin and even the parity is unknown and as for a given orbital angular momentum the correction factors K are not strongly spin-dependent, only averaged values for p- and d-wave resonances are given in Table IV, where the resulting correction factors K are summarized. It can be seen that the correction is  $\sim 5\%$  for measurements on  $^{56}\text{Fe}$  while they increase up to  $10\%$  for measurements on  $^{58}\text{Ni}$ . The correction factors are similar for s- and d-waves, as the respective capture gamma-ray spectra have about the same shape (see Sec. VII). In contrast, strong differences are observed for the p-wave correction factors. For given orbital angular momentum but different spins the results differed on the average only by  $0.5\%$ . Therefore they are not specified separately in Table IV. It has to be noted that the strong soft component in the gold spectra causes a non-negligible correction for the bismuth-graphite converter for which the linearity of the efficiency is assumed to hold very well above 1 MeV.

#### IV. RESULTS

The parameters for the s-wave resonances in  $^{58,60}\text{Ni}$  and  $^{56}\text{Fe}$  as obtained from the FANAC fits are compiled in Tables V to VII. These values are not yet corrected for the different efficiency of the individual detectors. The results from the two different evaluations, taking  $\Gamma_n$  as free or fixed parameter, are quoted separately. The statistical uncertainties which are calculated by the FANAC code are given in brackets. The code multiplies the uncertainty deduced from the error bars of the individual points by the so called error adjustment factor  $\chi$ . This factor is calculated as the square root of  $\chi^2$  obtained in the fit, divided by the number of data points minus number of free parameters. Thus, the uncertainty is increased if the fit is not able to reproduce the data points completely. As can be seen from the Tables, in most fits  $\chi \sim 1$  was obtained but in a few

cases only values of  $\chi \sim 1.2$  to  $1.3$  could be reached.

In Tables VIII to X the respective results for unresolved multiplets of p-wave resonances are given. As these data will only be used as a check for the experimental method we renounce to quote the statistical accuracy. From Figs. 5 to 9, however, it can be seen that it is compatible with the accuracy of s-wave resonances and therefore small compared to systematic uncertainties.

The fact that no systematic differences are observed in the results of one detector in the individual Runs confirms that the effects of sample thickness and neutron spectrum are accounted for correctly. Therefore, in further evaluation averages over all Runs are used. In case of s-wave resonances it proved that the mean value of both evaluation methods should be used (see discussion of individual isotopes below).

In Table XI and XII the data are corrected for detector efficiency using the correction factors K given in Table IV. This strongly reduces the spread in the data obtained with different detectors which now agree within their remaining statistical and systematic uncertainty. There is an indication that the data obtained with the bismuth graphite converter are systematically higher than the results of the two other detectors. The most probable explanation is the uncertainty in the shape of the efficiency curve for this detector. However, these differences can be tolerated in view of the systematic uncertainty of the efficiency correction (see Sec. V).

In the last columns of Table XII the final values for the capture widths of the investigated s-wave resonances are given together with their statistical and systematic uncertainties. These values are obtained as an average of the results from the individual detectors. In case of  $^{60}\text{Ni}$  the contribution of the two p-wave resonances at 12.2 and 13.6 keV is subtracted because it could not be separated in the fits. The results for the individual isotopes are discussed in detail below and the calculation of the systematic uncertainties will be given in Sec. V. For completeness we include in Table XII the result for  $^{56}\text{Fe}$  obtained

in our first experiment where we used three different sample thicknesses but only one Moxon-Rae detector (with graphite converter, Ref. 1). In Ref. 1 a correction for detector efficiency was not applied as no reliable capture gamma-ray spectra were available at that time. The value given in Table XII is now corrected according to Table IV and thus supersedes the earlier result.

<sup>58</sup>Ni: Evaluation 1 (taking  $\Gamma_n$  as a free parameter) tended to increase the neutron width of the s-wave resonance by inclusion of part of the area of the two p-wave resonances at 13.4 and 13.6 keV. We obtained an average neutron width  $\Gamma_n = 1.6$  keV (see Table V) whereas the average  $g\Gamma_\gamma\Gamma_n/\Gamma = 1.24$  eV of the two p-wave resonances is rather small (see Table VIII). In contrast, evaluation 2 with  $\Gamma_n = 1.32$  keV as a fixed parameter yielded  $g\Gamma_\gamma\Gamma_n/\Gamma = 1.34$  eV for the two p-wave resonances. Nevertheless, both values are in good agreement with the data which are reported in Refs. 13 and 20 for these two p-wave resonances (1.13 eV and 1.27 eV, respectively). Therefore, the mean of both evaluations was taken as final result and the spread was used to estimate the systematic uncertainty of the separation between s- and p-waves. The results for the two unresolved multiplets of p-wave resonances around 20 and 26 keV are systematically larger by 20-30 % than the data from literature <sup>13,20</sup>.

The final value  $\Gamma_\gamma = 1.53$  eV  $\pm$  6.6 % for the s-wave resonance at 15.35 keV is in good agreement with the KEDAK evaluation of Fröhner <sup>13</sup> but is lower by  $\sim$  35 % than the data given in Refs. 15 and 20. However, the results of Ref. 20 were not yet properly corrected for neutron sensitivity. A reevaluation of these data at Oak Ridge <sup>3</sup> yielded a preliminary value of  $\Gamma_\gamma = 1.3 \pm 0.4$  eV in agreement with our value. But it has to be pointed out that the neutron sensitivity of the respective experimental setup limits the accuracy of this resonance parameter to  $\sim$  15 % in the tank measurement performed at KfK (Ref. 13) and to  $\sim$  30 % in the measurement with the C<sub>6</sub>F<sub>6</sub> detector at Oak Ridge (Refs. 3 and 20). Compared to that the present method provides a significant improvement.

<sup>60</sup>Ni: For this isotope the two weak p-wave resonances at 12.2 and 13.6 keV could not be resolved from the area of the s-wave resonance. Therefore, in Table VI always the sum of the three resonances is quoted. The two evaluation methods agree within 1 % since a decrease in the resonance area of the s-wave resonance is compensated for by an increase in the p-component. The p-component differed on the average by a factor of two and was  $\sim 0.3$  eV if  $\Gamma_n$  is taken as a free parameter and  $\sim 0.6$  eV if  $\Gamma_n$  is taken as fixed.

To obtain the final value for the capture width of the s-wave resonance the value  $g\Gamma_\gamma\Gamma_n/\Gamma = 0.56$  eV of Ref. 13 was subtracted from the observed area. This value is in very good agreement with the recent results of Perey et al.<sup>2</sup> who quote  $g\Gamma_\gamma\Gamma_n/\Gamma = 0.554$  eV. Our final value for the s-wave resonance  $\Gamma_\gamma = 2.92$  eV  $\pm 6.6$  % is in good agreement with the KEDAK evaluation<sup>13</sup> (2.73 eV) and with the new results from Oak Ridge<sup>2</sup> (2.6 eV). But, again, these data carry uncertainties of 18 % and 34 %, respectively. The value in Ref. 15 which is based on the work of Stieglitz et al.<sup>21</sup> is  $\sim 15$  % larger than the present value. The results for the unresolved multiplets of p-wave resonances are in good agreement with the data of Refs. 13 and 2.

<sup>56</sup>Fe: Even with the limited resolution of the present experiment, this resonance is undisturbed by any p-wave contribution. The results obtained with the two evaluation methods agree on the average within 2 % except for the graphite converter where a significantly larger  $\Gamma_n$  value was obtained in the fit. The final result for the 27.7 keV s-wave resonance (see Table XII) agrees very well with our extensive measurements published already in Ref. 1, if properly corrected for the detector efficiency. Thus our measurements with Moxon Rae detectors yielded a consistent final value of  $\Gamma_\gamma = 1.06 \pm 0.05$  eV for this resonance using samples which differ by more than a factor of 10 in thickness. This is an impressive confirmation of the multiple scattering correction of the FANAC code. There is also excellent agreement with the value  $\Gamma_\gamma = 1.04 \pm 0.08$  eV obtained recently at Karlsruhe<sup>22</sup> in a measurement using  $C_6D_6$  detectors and a flight path of 60 cm. The present value is significantly lower than all results published before 1980

(Refs. 23 to 25), except the result of Fröhner<sup>13</sup> who quoted  $\Gamma_\gamma = 1.25 \pm 0.2$  eV. We also agree with the result from a measurement at Geel<sup>6</sup>, which was analysed by Moxon using the REFIT code<sup>26</sup> ( $\Gamma_\gamma = 1.0$ ). Recently, a new measurement was published<sup>27</sup> which yielded a significantly lower value  $\Gamma_\gamma = 0.82$ . This result is correlated with a surprisingly low value for the neutron width of this resonance ( $\Gamma_n = 1.15$  keV). Low values for  $\Gamma_\gamma$  are also reported by Gayther et al.<sup>28</sup> ( $\Gamma_\gamma = 0.85$  eV) and by Allen et al.<sup>9</sup> ( $\Gamma_\gamma = 0.82 \pm 0.11$  eV). For the unresolved multiplet of p-wave resonances around 36 keV we found a total area of  $g\Gamma_\gamma\Gamma_n/\Gamma = 1.25$  eV in the present experiment and  $g\Gamma_\gamma\Gamma_n/\Gamma = 1.17$  eV after correction of the results from Ref. 1. This is in good agreement with our data obtained with  $C_6D_6$  detectors (1.21 eV) as well as with the data given by Fröhner<sup>13</sup> (1.19 eV) and Corvi et al.<sup>27</sup> (1.19 eV).

## V. DISCUSSION OF UNCERTAINTIES

The evaluation of the systematic uncertainties of the present experimental method is discussed in detail in Ref. 1. The individual components which are compiled in Table XIII have been determined from the spectra measured with the graphite converter. As no significant difference is observed to the respective spectra measured with the two other detectors (see Fig. 2) they are representative for the whole experiment.

### V A Statistical Uncertainty.

The statistical uncertainty of each TOF channel is given by  $(C_{\text{effect}} + C_{\text{backgr.}})^{1/2}$ .  $C_{\text{effect}}$  is the count rate measured with the respective sample and  $C_{\text{backgr.}}$  is the sum of all subtracted background components. The uncertainty in the capture yield used as input for the FANAC fits, was calculated by quadratic summation of the uncertainties in the measured spectra for the isotope and the gold sample. The values quoted in Tables V to VII are directly taken from the output of FANAC. They are already multiplied by the error adjustment factor  $\chi$ .

As the uncertainties are comparable in the individual Runs we renounced on calculating a weighted average from the individual data. Instead, the uncertainty for the averaged values is simply the mean of the individual uncertainties divided by the square-root of the number of measurements.

In  $^{58}\text{Ni}$ , the statistical uncertainty in the fits obtained with evaluation method 1 ( $\Gamma_\gamma$  free) exceeds the one from method 2 ( $\Gamma_\gamma$  fixed) by  $\sim 50\%$ . This is because by method 2 a larger capture area and hence a larger part of the statistical uncertainty is assigned to the overlapping p-wave resonances. For the mean value of  $\Gamma_\gamma$  from both evaluation methods the average of the respective statistical uncertainties was used.

In case of  $^{60}\text{Ni}$  the quoted uncertainties are significantly larger than the preliminary data given in Ref. 29 where we missed to include the absolute statistical uncertainty by the two weak p-wave resonances at 12.2 and 13.6 keV.

#### V B Systematic Uncertainties of the Capture Yield.

-----

The following systematic uncertainties of the capture yield have been considered:

- 1.) Flight path transformation: The measured flight path was assumed to have a remaining uncertainty of  $\pm 0.3$  mm. In the transformation of the individual TOF spectra to a common flight path this leads to an uncertainty in solid angle and to an uncertainty in the transformation of the time scale as well. In the first evaluation given in Ref. 1 the latter component was estimated from the relative change of the count rate in the individual TOF channels if the spectrum is transformed according to a  $\pm 0.3$  mm different flight path. However, this procedure yields an overestimate for the uncertainty since the transformation causes a shift of the resonance, thus changing the count rate on the left and right wing in opposite directions. Indeed, the resonance area itself is almost unchanged in the transformation and the corresponding uncertainty quoted in Table XIII is dominated by the uncertainty in solid angle.

- 2.) Constant background: This uncertainty was determined from the scatter of the results if three different TOF regions were used for background determination. This uncertainty is correlated to the statistical accuracy of the measured spectra and the corresponding background. It is therefore the smallest in Run III with the longest measuring time.
- 3.) Neutron beam intensity: The uncertainty for the flux normalization was estimated from the differences which are obtained if this normalization is calculated from the spectra of the transmission detector or of the neutron flux monitor. As a TOF spectrum is used in the first case and an analogue spectrum in the second, both procedures are widely independent and thus the observed differences are a reasonable estimate for the uncertainty. The influence of the energy dependence of the neutron flux on the data was discussed in Ref. 1 where the correlated uncertainty was found to be negligible.
- 4.) Correction for multiple scattering and self-shielding in the gold sample: This uncertainty is the same as discussed in Ref. 1.
- 5.) Gamma-ray self-absorption: As can be seen from Table I this correction cancels out to a large extent in a relative measurement. Only for the 2 mm iron sample it had to be applied; in all other cases it is smaller than the quoted uncertainty of 1 %.
- 6.) Gold standard cross section: An uncertainty of 2.5 % was assumed for the ENDF/B-V standard cross section. This seems to be somewhat optimistic if one considers that the data of Macklin et al.<sup>10</sup> have recently been changed by 3.3 % at 10 keV<sup>11</sup>. On the other hand new values for the gold standard are easily implemented in the evaluation. The influence of structure in the gold standard on the measured data is discussed in Ref. 1 and contributes no significant additional uncertainty.

V C Systematic Uncertainties for the Calculations with  
the FANAC Code.

-----

In Ref. 1 an uncertainty of 2 % was deduced for the FANAC fit, considering uncertainties in multiple scattering and in the fixed input parameters. An additional uncertainty of 1 % is taken into account in the present evaluation as the resonance energies are determined with an accuracy of only  $\sim 1$  % (see Tables V to VII) which propagates directly to the respective value for  $\Gamma_{\gamma}$ .

An additional uncertainty was considered for the subtraction of the p-wave component in  $^{58,60}\text{Ni}$ . For  $^{58}\text{Ni}$  an uncertainty of 3 % seemed to be a reasonable estimate as the two evaluation methods are extreme cases for this subtraction. For  $^{60}\text{Ni}$  an uncertainty of 10 % was estimated for the subtracted p-wave component which is certainly conservative in view of the  $\sim 5$  % accuracy quoted in Ref. 2 for the p-wave resonances at 12.2 and 13.6 keV and the good agreement between Ref. 2 and KEDAK <sup>13</sup>.

V D Systematic Uncertainty of the Efficiency Correction

-----

The systematic uncertainty of the efficiency correction as given in Table XIII is composed of three parts.

- a.) The uncertainty correlated with the shape of the efficiency curve  $\epsilon(E_{\gamma})$ : This part was estimated from the difference by calculating the K values with two different shapes for the graphite converter as shown in Fig. 10. The resulting differences are 3.7 %, 2.7 % and 1.8 % for  $^{58,60}\text{Ni}$  and  $^{56}\text{Fe}$ , respectively, and were assumed as uncertainties.
- b.) The uncertainty due to the shape of the capture gamma ray spectrum of gold: This part was estimated to 0.5 % from a comparison of the results obtained in Ref. 19 with the theoretical spectrum and the measured spectra.
- c.) The uncertainty due to the shape of the capture gamma-ray spectrum of the s-wave resonances: This part is dominated

by the uncertainty of the bin with highest energy in the gamma spectrum (see Fig. 12). As outlined in Sec. VII this bin contains only gamma transitions to the ground state and the first excited state in the respective compound nucleus. Therefore, the correlated intensity is rather uncertain as for a single resonance it follows essentially a Porter Thomas distribution with a low effective number of degrees of freedom. Fortunately, there exist measurements of Beer et al. <sup>45</sup> for the involved partial widths. As shown in Sec. VII the agreement between the calculation (including a valence contribution and an interference term) and the experiment is 40 %, 3 % and 30 % for <sup>58,60</sup>Ni and <sup>56</sup>Fe, respectively. We assumed an uncertainty of 50 % for the intensity in the highest bin for <sup>58</sup>Ni and <sup>56</sup>Fe and 25 % for <sup>60</sup>Ni. This resulted in a 0.8 % uncertainty for the respective K-values. If we add a 0.5 % uncertainty correlated to the shape of the remaining bins (comparable to the uncertainty in the gold spectrum) we end up with a 1 % uncertainty for that last part.

## VI AVERAGE CROSS SECTIONS

The importance of accurate values for  $\Gamma_\gamma$  of the investigated s-wave resonances are illustrated at the example of design studies for a typical fast breeder power reactor. In addition, Maxwellian average cross sections have been determined, which are of importance for nuclear astrophysics.

### VI A Fast Reactor Spectrum Averaged Cross Sections

To study the influence and importance of the present results for an actual reactor we chose the core design studies for the SNR-2 power reactor by Kiefhaber <sup>30</sup>. For the purpose of the intended comparison a one dimensional representation seemed sufficient, assuming a constant neutron flux for the whole core, grouped into 26 energy bins. About 12 % of the total capture rate

is due to capture in structural materials. The bulk of this rate is due to capture in iron (50 %) and nickel (22 %), while the rest is caused by chromium, molybdenum and niobium. In all involved materials neutron capture proceeds via the  $(n,\gamma)$ -reaction with the exception of nickel where one third of the capture events is attributed to the  $(n,p)$  reaction because of the low threshold energy.

In each energy group an average capture cross section was determined by lumping together the resonance areas of the individual resonances: Here we used the data from KEDAK (Ref.13) for  $^{56}\text{Fe}$  and  $^{58}\text{Ni}$  and from Ref. 2 for  $^{60}\text{Ni}$  and our own values for the s-wave resonances. Above 200 keV smoothed cross sections were taken from Ref. 31. These cross section were weighted with the neutron flux of the respective group. This procedure was performed twice, with and without the measured s-wave resonance. The resulting contributions of the s-wave resonances to the total capture rate of the respective isotopes are given in Table XIV in comparison the values obtained with the s-wave resonance parameters quoted by Mughabghab et al. (Ref. 15). From this Table the following conclusions can be drawn:

- 1.) About 9 % of the total capture rate in structural materials is caused by the three investigated resonances.
- 2.) Using the present data the capture rate in structural materials is reduced by more than 2 %.
- 3.) With the improved accuracy of  $\sim 5 - 6$  % of the present experiment the uncertainty in capture rate of structural materials is not any longer dominated by the uncertainty of the s-wave resonances. The main uncertainty is now determined by the 1.15 keV resonance in  $^{56}\text{Fe}$ , which contributes  $\sim 35$  % to the capture rate in  $^{56}\text{Fe}$ .
- 4.) Finally, one has to keep in mind that all other s-wave resonances as measured in previous experiments have been overestimated, too. If this is corrected a further reduction of the capture rate in structural materials is expected.

## VI B Maxwellian Average Cross Sections

---

For the investigation of element synthesis by the s-process <sup>32</sup> neutron capture cross sections are required as input data. As the helium burning shell of Red Giant Stars is commonly considered as the site for the s-process, this means that one must assume a Maxwellian neutron energy distribution for a thermal energy of  $kT \sim 30$  keV corresponding to a mean temperature between 300 and 400 million K. According to the conventions in the literature <sup>33</sup> the effective average cross section in such a scenario is given by

$$\frac{\langle \sigma v \rangle}{v_T} = \frac{1}{v_T} \int_0^{\infty} \sigma(v) v \phi(v) dv,$$

where  $\phi(v)$  is the Maxwellian velocity distribution. The thermal velocity  $v_T = (2 kT/m)^{1/2}$  is expressed by the temperature and the reduced mass  $m$ . Due to the shape of the Maxwellian velocity distribution, the limits of integration can be restricted to the energy range between 1 and  $\sim 200$  keV.

For resonant cross sections eq. (3) can be replaced by <sup>34</sup>

$$\frac{\langle \sigma v \rangle}{v_T} = \sigma_{th} \left( \frac{25.3 \cdot 10^{-6}}{kT} \right)^{1/2} + \frac{2}{\sqrt{\pi}} \sum_r A_r \frac{E_r}{(kT)^2} \exp\left(-\frac{E_r}{kT}\right)$$

where the first term accounts for the effect of distant resonances,  $\sigma_{th}$  being the capture cross section at  $kT = 0.0253$  eV.  $A_r$  is the resonance area and  $E_r$  the resonance energy.

In Table XV the results for the Maxwellian average cross section of <sup>58</sup>Ni and <sup>60</sup>Ni are given. The parameters of the s-wave resonances were taken from the present work. In case of <sup>58</sup>Ni all other values for  $\Gamma_\gamma$  were taken either from Ref. 13 or from Ref. 20. The quoted value is an average of both results. In case of <sup>60</sup>Ni the values of Ref. 2 were used. The accuracy given for <sup>58</sup>Ni was derived from the spread of the results as obtained with the two different data sets. In case of the Maxwellian averaged cross section of <sup>60</sup>Ni a 4 % systematic uncertainty and a 2 % statistical uncertainty was assumed for the data of Ref. 2.

The contribution of the s-wave resonances to the averaged cross section is quoted in Table XV separately. This demonstrates that without an accurate value for these resonances no reliable result for the Maxwellian average cross section can be given. A value for  $^{56}\text{Fe}$  has been published already in Ref. 22. This result remains unchanged as the same value for the 27.7 keV resonance was observed in the present work.

## VII. CALCULATION OF CAPTURE GAMMA-RAY SPECTRA

In order to estimate the gamma-ray spectrum of the compound nucleus decay we adopted the same codes and methods already outlined in Refs. (16, 19, 35). In the present case, in particular, it was necessary to determine the gamma-ray spectrum for the 27.7, 15.4, 12.5 keV s-wave resonances in  $^{56}\text{Fe}$ ,  $^{58,60}\text{Ni}$ , respectively. In addition to the usual compound nucleus contribution we have considered a valence contribution as well as the corresponding interference term. In the calculations M1 contributions were included as they were found to be of importance especially for p-wave resonances.

As far as the valence contributions are concerned they have been estimated according to the same method and with the same parameters as are given in Ref. 36. Where the primary gamma decay was due to valence transitions to excited levels the following complete gamma-ray cascade was accounted for. Dealing with resonance capture total and partial cross sections were calculated in terms of the Breit-Wigner formula in order to sum the contributions from all capture mechanisms consistently.

Similarly, also the corresponding integrated spectra were normalized to the peak cross sections. The compound nucleus parameterization is listed in Table XVI. The observed mean level spacing,  $D_{\text{OBS}}$ , has been guessed from the work of Refs. 14, 37, 38, 39 and from systematics. The deformation parameter  $\beta$  for  $^{57}\text{Fe}$  was interpolated from Ref. 40. For  $^{61}\text{Ni}$  it was taken from Ref. 41 and for  $^{59}\text{Ni}$  it was guessed to be the same as for  $^{61}\text{Ni}$ . The giant resonance parameters  $E_i$ ,  $\Gamma_i$ ,  $\sigma_i$  were determined as a function of  $\beta$  by means of the systematics in

Ref. 42. The level density parameters  $a$ ,  $U_x$ ,  $T$  and  $\sigma^2$  were derived in the usual way<sup>19,35,42</sup> from  $D_{OBS}$  and from the analysis of the discrete levels as illustrated in Fig. 11. The adopted level schemes are given in Table XVII.

In Table XVIII we give calculated average values of total s- p- and d-wave radiative widths  $\Gamma_\gamma^{J,\pi}$  for both spin states together with the variance of their respective theoretical  $\chi^2$ -distributions,

$$\sigma = \sqrt{\frac{2}{\nu_{eff}} \langle \Gamma_\gamma \rangle}$$

with the effective number of degrees of freedom,  $\nu_{eff}$ , as defined in Refs. 36,45. Average experimental values are included for comparison. The M1 contribution is also given in terms of the Axel model with giant resonance parameters  $E_R$ ,  $\Gamma_R$  and  $\sigma_R$  as quoted in Table XVI. (The valence contribution to M1 transitions was found to be negligible).

In Table XIX our results are summarized by quoting the following values:

- $E_\lambda$  : resonance energy
- $E_{LEVEL}$  : discrete level in the compound nucleus
- $\Gamma_\lambda^O$  : neutron width
- $\Gamma_\gamma^{STAT}$  : statistical contribution to total radiative width
- $\sigma^{STAT}$  : cross section of the statistical contribution at the resonance peak
- $\Gamma_\gamma^{VAL}$  : valence contribution to total radiative width
- $\sigma^{TOT_1}$  : cross section of the statistical and valence contribution at the resonance peak
- $\Gamma_\gamma^{TOT}$  : total radiative width as a sum of the statistical and valence contribution with inclusion of an interference term.
- $\sigma^{TOT_2}$  : cross section of the statistical and valence contribution with the inclusion of an interference term at the resonance peak.
- $\Gamma_\gamma^{EXP}$  : experimental total and partial capture widths.

In particular, we list separately the compound nucleus contribution and the compound nucleus plus valence contribution. We also give the total capture cross section under the assumption of an interference term the sign of which was established a posteriori from the fit of experimental total and partial radiative widths (Ref. 45). We are aware that this procedure is only tentative, considering the high uncertainty coming from statistical fluctuation. The method can not be taken as a proof of the agreement, it only gives an idea of the size of the interference effect. The calculated spectra are shown in Fig. 12. Obviously, the inclusion of a valence and an interference term affects the spectra significantly.

The cross section is correlated to the radiative width through the Breit-Wigner formula. In splitting the radiative width in its components we have to remind that as far as the compound nucleus part is concerned we can only calculate an average value. Consequently, it is observed that the calculated average value for single transitions as well as for the contributions lumped into the spectrum bins, may be very different from measured values. In particular, this holds for the last two or three bins in the harder tail of the spectrum which are feeded only by a few primary transitions to the first excited states in the compound nucleus. Then, the effective number of degrees of freedom is very low, namely close to the number of contributing levels, and a large variance is expected for the calculated average values. This is shown in the fourth column of Table XIX were brackets group transitions which are lumped together in one bin of the gamma ray spectrum, respectively. The quoted percentages are the inherent standard deviations due to the statistical fluctuations of the lumped widths. In our case, by chance, we happen to find total and partial radiative widths pretty consistent with experimental measurements thus confirming the high energy tail of our spectra. Because the fluctuations greatly decrease for secondary transitions as well as for the softer primary transitions (due to a rapidly increasing number of transitions falling into the individual bins) we are confident that - on the whole - the remaining part of our calculated spectra are

not too much affected by fluctuations. Differently, the valence contributions do not exhibit such ambiguities because the neutron widths to which they are correlated are known for all investigated resonances. As long as the relative valence contribution is small, the total capture cross section fluctuates in the same way as the compound nucleus component. This is the case for all resonances considered here. In order to keep the fluctuation effects as small as possible we chose the most coarse energy grid for the capture gamma-ray spectra compatible with the purpose of the experiment.

Spectra for each spin of p- and d-wave neutrons averaged over all resonances have also been calculated in order to correct properly for  $l \neq 0$  resonances observed in the measurement. Because for a given angular momentum  $l$  the spectra are not sensitive to the spin, Fig. 13 shows only the sum of the spectra for the two possible spin states. However, for different  $l$ -waves there are significant differences in the spectra which are caused by the parity distributions of the low lying levels. The first 10 or 12 levels in all compound nuclei have negative parity (see Table XVII) and are therefore reached via E1 transitions following s- or d-wave capture, thus favouring the hard and soft component in the respective capture gamma-ray spectra. Capture of p-wave neutrons populates negative parity states in the compound nuclei which cannot easily decay to the low lying states by direct E1 transitions and therefore the related gamma-ray spectra exhibit a rather smooth behaviour, even if M1 contributions are included as can be understood from the composition of E1 and M1 contributions, respectively (see Table XVIII). For completeness we quote in Table XX the average capture cross section of s-, p- and d-wave resonances in dependence of the gamma ray multiplicity. It can be seen from this table that on the average the gamma ray multiplicity of the capture cascades is significantly larger for p-waves than for s- and d-waves.

ACKNOWLEDGEMENTS

We would like to thank A. Ernst and D. Roller for the continuous support in providing optimum beam conditions. In addition we appreciated very much the help of G. Rupp in optimizing the experimental setup.

REFERENCES

- 1.) K. WISSHAK and F. KÄPPELER, Nucl. Sci. Eng. 77, 58 (1981)
- 2.) C.M. PEREY, J.A. HARVEY, R.L. MACKLIN, R. R. WINTERS, and F.G. PEREY, "Neutron Transmission and Capture Measurements and Analysis of  $^{60}\text{Ni}$  from 1 to 450 keV, ORNL-5893, ENDF-330 Oak Ridge National Laboratory November 1982
- 3.) C.M. PEREY, Private Communications 1982
- 4.) N. DAYDAY, Ed. "World Request List for Nuclear Data", INDC (SEC) - 78 / URSF International Atomic Energy Agency, Vienna 1981
- 5.) D.B. GAYTHER, B.W. THOMAS, B. THOM, and M.C. MOXON, Proc. Specialists' Meeting Neutron Data of Structural Materials for Fast Reactors, Geel, Belgium, December 5-8, 1977, Pergamon Press, Oxford (1979) p. 547
- 6.) A. BRUSEGAN, F.CORVI, G. ROHR, R. SHELLY, and T. VAN DER VEEN, Proc. Conf. Nuclear Cross Sections and Technology, Knoxville, Tenn., October 22-26, 1979, NBS Spec. Publ. 594, National Bureau of Standards.
- 7.) R.L. MACKLIN, J.H. GIBBONS, and T. INADA Nucl. Phys. 43 353 (1963)
- 8.) L. PAGES, E. BERTEL, H. JOFFRE, and L. SKLAVENITIS, Atomic Data 4, 1 (1972)
- 9.) B.J. ALLEN, D.D. COHEN, and F.Z. COMPANY, J. Physics G: Nucl. Phys. 6, 1173 (1980)
- 10.) R.L. MACKLIN, J. HALPERIN, and R.R. WINTERS, Phys. Rev. C 11, 1270 (1975)
- 11.) R.L. MACKLIN private Communications 1982
- 12.) F.H. FRÖHNER, "FANAC - A Shape Analysis Program for Resonance Parameter Extraction from Neutron Capture Data for Light- and Medium Weight Nuclei", KfK-2145, Kernforschungszentrum Karlsruhe (1977)
- 13.) F.H. FRÖHNER, Proc. of a Specialists Meeting on Neutron Data of Structural Materials for Fast Reactors, Geel 5-8 December 1977, Pergamon Press Oxford (1979) p.138

- 14.) F.H. FRÖHNER, K. WISSHAK, and F. KÄPPELER, "Recent Work on Structural Material Cross Sections at Kernforschungszentrum Karlsruhe", KfK 2899 Kernforschungszentrum Karlsruhe 1979
- 15.) S.F. MUGHABGHAB, M. DIVADEENAM, and N.E. HOLDEN, Neutron Cross Sections Vol. I  
Neutron Resonance Parameters and Thermal Cross Sections Part A, Academic Press New York 1981
- 16.) G. REFFO, F. FABBRI, K. WISSHAK, and F. KÄPPELER  
Nucl. Sci. Eng. 83, 401 (1983)
- 17.) S.S. MALIK and C. F. MAJKRZAK,  
Nucl. Instr. Methods 130, 443 (1975)
- 18.) K.V.K. IYENGAR, B.LAL and M.L. JHINGAN  
Nucl. Instr. and Methods 121, 33 (1974)
- 19.) G. REFFO, F. FABBRI, K. WISSHAK, and F. KÄPPELER,  
Nucl. Sci. Eng. 80 630 (1982)
- 20.) F.G. PEREY, G.T. CHAPMAN, W.E. KINNEY and C.M. PEREY,  
Proc. of a Specialists Meeting on Neutron Data of Structural Materials for Fast Reactors, Geel 5-8 December 1977, Pergamon Press Oxford (1979) p. 530
- 21.) R.G. STIEGLITZ, R.W. HOCKENBURY and R.C. BLOCK,  
Nucl. Phys. A163, 592 (1971)
- 22.) F. KÄPPELER, K. WISSHAK, and L.D. HONG, Nucl. Sci. Eng.  
in print
- 23.) R.L. MACKLIN, P.J. PASMA, and J.H. GIBBONS, Phys. Rev.  
B136, 695 (1964)
- 24.) R.W. HOCKENBURY, Z.M. BARTOLOME, J.R. TATARCZUK, W.R. MOYER,  
and R.C. BLOCK, Phys. Rev. 178, 1746 (1969)
- 25.) B.J. ALLEN, A.R. de L. MUSGROVE, J.W. BOLDEMAN, and  
M.J. KENNY, Nucl. Phys. A 269, 408 (1976)
- 26.) M.C. MOXON, "Nuclear Physics Division Progress Report 1980",  
AERE-PR/NP 28 United Kingdom Atomic Energy Authority  
Harwell 1981

- 27.) F. CORVI, A. BRUSEGAN, R. BUYL, G. ROHR, R. SHELLEY,  
and T. VAN DER VEEN, Proc. Int. Conf. on Nuclear Data  
for Science and Technology, Antwerp 6-10 September 1982
- 28.) D.B. GAYTHER, M.C. MOXON, R.B. THOM, and J.E. JOLLY,  
"U.K. Nuclear Data Progress Report 1979",  
UKNDC (80), P. 96, NEANDC (E) 212, Vol. 8, United Kingdom  
Atomic Energy Authority Harwell 1980
- 29.) K. WISSHAK, F. KÄPPELER, G. REFFO, and F. FABBRI, Proc.  
of a Specialists Meeting on Fast Neutron Capture,  
Argonne 20-23 April 1982
- 30.) E. KIEFHABER, private Communications 1983
- 31.) C.LE. RIGOLEUR, A. ARNAUD, and J. TASTE, Mesures en  
Valeur Absolue des Sections Efficaces de Capture Radiative  
des Neutrons par le  $^{23}\text{Na}$ , Cr,  $^{55}\text{Mn}$ , Fe, Ni,  $^{103}\text{Rh}$ , Ta,  $^{197}\text{Au}$ ,  
 $^{238}\text{U}$  dans le Domaine de 10 à 600 keV", CEA-R-4788  
Commissariat à l'Energie Atomique 1976
- 32.) P.A. SEEGER, W.A. FOWLER, and D.D. CLAYTON,  
Ap. J. Suppl. 11, 121 (1965)
- 33.) D.D. CLAYTON, W.A. FOWLER, T.E. HULL, and B.A. ZIMMERMAN,  
Annals. Phys. 12, 331 (1961)
- 34.) B.J. ALLEN, R.L. MACKLIN, and J.H. GIBBONS,  
Adv. Nucl. Phys. 4, 205 (1971).
- 35.) K. WISSHAK, J. WICKENHAUSER, F. KÄPPELER, G. REFFO,  
and F. FABBRI, Nucl. Sci. Eng. 81, 396 (1982)
- 36.) A. MENGONI, G. REFFO, and F. FABBRI, Proc. Int. Conf. on  
Nuclear Data for Science and Technology, Antwerp 6-10  
September 1982
- 37.) S. IIJIMA, H. YAMEKOSHI, N. SEKINE, Y. KIKUCHI, and T. ASAMI,  
NEANDC Topical Discussion on Neutron Data of Structural  
Materials, CBNM Geel, 26 September 1979
- 38.) S.F. MUGHABGHAB, and D.I. GARBER, Neutron Cross Sections,  
Vol. I, Neutron Resonance Parameters, BNL 325  
3rd ed., 1973, Brookhaven National Laboratory, Upton,  
New York

- 39.) G. ROHR, in Neutron Data of Structural Materials for Fast Reactors, K.H. Böckhoff, ed. Pergamon Press, Oxford (1979) p. 614
- 40.) P.H. STELSON, and L. GRODZINS, Nucl. Data Sect. A, 1, 21 (1965)
- 41.) G.H. FULLER, and V.W. COHEN, Nucl. Data Tables A5, 433 (1969)
- 42.) G. REFFO, in Nuclear Theory for Applications, IAEA-SMR 43, International Atomic Energy Agency Vienna (1980)
- 43.) C.M. LEDERER, and V.S. SHIRLEY, Tables of Isotopes, 7th ed., John Wiley & Sons, Inc. New York (1978)
- 44.) H. GRUPPELAR and G. REFFO, Nucl. Sci. Eng. 62, 756 (1977)
- 45.) H. BEER, R.R. SPENCER, and F. KÄPPELER  
Zeitschrift für Physik A 284, 173 (1978)

Table I Compilation of the Relevant Sample Data

Sample	Chemical Composition	Isotopic Composition (%)	Weight (g)	Thickness (atom/b)	Thickness (mm)	Multiple Scattering in s-Wave in % of primary capture events	Gamma Ray Self-Absorption SA
$^{58}\text{Ni}$	Metal	99.76 (58)	4.525	$4.100 \times 10^{-3}$	0.45	79	0.991
		0.21 (60)	2.993	$2.712 \times 10^{-3}$	0.30	54	0.994
		0.01 (61)	1.532	$1.388 \times 10^{-3}$	0.15	30	0.997
		0.02 (62)					
		$\leq 0.02$ (64)					
$^{60}\text{Ni}$	Metal	0.81 (58)	4.706	$4.122 \times 10^{-3}$	0.45	113	0.991
		99.08 (60)	3.168	$2.775 \times 10^{-3}$	0.30	75	0.994
		0.05 (61)	1.538	$1.347 \times 10^{-3}$	0.15	41	0.997
		0.07 (62)					
		$\leq 0.02$ (64)					
$^{56}\text{Fe}$	Metal	0.03 (54)	2.827	$2.653 \times 10^{-3}$	0.30	22	0.995
		99.93 (56)					
		0.03 (57)					
		$\leq 0.02$ (58)					
$^{56}\text{Fe}$	Metal	natural	17.24	$1.622 \times 10^{-2}$	2.0	89	0.969
$^{197}\text{Au}$	Metal	natural	5.089	$1.358 \times 10^{-3}$	0.25	1.024 <sup>a)</sup>	0.988
C	Graphite	natural	1.729	$7.571 \times 10^{-3}$	0.9	-	-

Sample Diameter: 38.2 mm

a) Correction for multiple scattering and self-shielding

Table II Important Parameters of the Individual Measurements.

Run	Sample 1	Sample 2	Flight Path (mm)	Neutron Energy Range (keV)	Measuring Time per Sample (h)
I	$^{58}\text{Ni}$ (0.45 mm)	$^{60}\text{Ni}$ (0.45 mm)	87.7	5 to 90	13.8
II	$^{58}\text{Ni}$ (0.30 mm)	$^{60}\text{Ni}$ (0.30 mm)	87.8	7 to 75	22.6
III	$^{58}\text{Ni}$ (0.15 mm)	$^{60}\text{Ni}$ (0.15 mm)	87.7	10 to 60	57.6
IV	$^{58}\text{Ni}$ (0.45 mm)	$^{60}\text{Ni}$ (0.45 mm)	88.0	10 to 60	18.1
V	$^{56}\text{Fe}$ (0.3 mm)	$^{56}\text{Fe}$ (2.0 mm)	89.0	10 to 60	38.6/6.5 <sup>a</sup>

<sup>a</sup> Sample 1 and 2, respectively

Table III Parameters Taken as Fixed Input Data for the Calculations with the FANAC Code

$^{58}\text{Ni}$				$^{60}\text{Ni}$				$^{56}\text{Fe}$			
				s-wave strength function ( $\times 10^{-4}$ )							
2.9				3.1				2.5			
				s-wave radius (fm)							
7.5				6.7				6.1			
				p-wave radius (fm)							
5.4				5.4				5.4			
				s-wave resonances							
$E_\gamma$ (keV)	$\Gamma_n$ (keV)	$\Gamma_\gamma$ (eV)		$E_\gamma$ (keV)	$\Gamma_n$ (keV)	$\Gamma_\gamma$ (eV)		$E_\gamma$ (keV)	$\Gamma_n$ (keV)	$\Gamma_\gamma$ (eV)	
15.35	1.320	-		12.5	2.66	-		-3.9	0.52	1.3	
63.1	3.6	2.3		28.6	0.8	-		27.7	1.4	-	
				43.0	0.12	-		74.0	0.54	0.63	
				65.1	0.6	-		83.7	1.3	0.5	
				86.6	0.33	1.5					
				p-wave resonances							
$E_\gamma$ (keV)	$\Gamma_n$ (eV)	$\Gamma_\gamma$ (eV)	g	$E_\gamma$ (keV)	$\Gamma_n$ (eV)	$\Gamma_\gamma$ (eV)	g	$E_\gamma$ (keV)	$\Gamma_n$ (eV)	$\Gamma_\gamma$ (eV)	g
13.4	3	-	1	12.2	1	-	1	22.7	-	0.6	3
13.6	3	-	2	13.6	1	-	2	34.2	1	-	2
17.5	1	0.007	3	17.2	1	0.02	3	36.7	3	-	1
19.0	1	-	1	23.9	3	-	1	38.3	-	0.6	2
20.0	1	-	2	28.5	1	0.05	2	45.9	10	-	1
21.1	3	-	3	29.5	1	0.01	3				
26.1	1	-	1	30.2	1	-	1				
26.6	3	-	2	33.0	3	-	3				

Table IV Efficiency Correction Factors K for  
Relative Measurement of Structural Materials  
to a Gold Standard Using Moxon Rae Detectors  
with Different Converter Materials

		Converter Material		
		Graphite	Bismuth- Graphite	Bismuth
$^{58}\text{Ni}$	s	1.084	0.955	0.883
	p	1.023	0.971	0.925
	d	1.087	0.956	0.883
$^{60}\text{Ni}$	s	1.084	0.965	0.883
	p	1.004	0.978	0.948
	d	1.053	0.972	0.907
$^{56}\text{Fe}$	s	1.039	0.978	0.922
	p	1.013	0.987	0.954
	d	1.068	0.990	0.923

Table V Results for the Capture Width of the s-Wave Resonance at 15.35 keV in  $^{58}\text{Ni}$   
not yet Corrected for Detector Efficiency <sup>a)</sup>

Run	Graphite Converter				Bismuth Graphite Converter				Bismuth Converter				
	$E_n$ (keV)	$\Gamma_n$ (keV)	$\Gamma_\gamma$ (eV)	$\chi^b$	$E_n$ (keV)	$\Gamma_n$ (keV)	$\Gamma_\gamma$ (eV)	$\chi^b$	$E_n$ (keV)	$\Gamma_n$ (keV)	$\Gamma_\gamma$ (eV)	$\chi^b$	
Evaluation 1: $\Gamma_n$ Free Parameter	I	15.58	2.01(13.)	1.31(8.4)	0.89	15.60	1.89(11.3)	1.92(6.9)	0.98	15.57	1.57(12.5)	1.80(7.4)	1.07
	II	15.33	1.59(15.)	1.42(9.0)	1.05	15.51	1.57(19.7)	1.67(11.9)	1.15	15.34	1.55(14.3)	1.77(8.9)	1.20
	III	15.42	1.36(10.5)	1.30(6.3)	0.80	15.61	1.65(12.2)	1.80(7.4)	0.91	15.42	1.51(11.3)	1.80(6.8)	1.06
	IV	15.36	1.61(15.2)	1.29(9.6)	1.32	15.54	1.41(8.5)	1.60(4.9)	0.76	15.36	1.67(11.2)	1.75(6.8)	1.07
	Average	15.42	1.64	1.33(4.2)		15.57	1.63	1.75(3.9)		15.42	1.58	1.81(3.7)	
Evaluation 2: $\Gamma_n$ Fixed Parameter	I	15.66	1.32	1.16(5.2)	1.01	15.68	1.32	1.80(5.4)	0.99	15.60	1.32	1.77(5.0)	1.08
	II	15.38		1.32(5.6)	1.07	15.54		1.59(7.0)	1.16	15.36		1.71(5.3)	1.07
	III	15.42		1.30(4.2)	0.95	15.66		1.64(4.2)	0.93	15.44		1.71(4.3)	1.06
	IV	15.37		1.25(5.8)	1.34	15.54		1.62(3.4)	0.75	15.38		1.70(4.8)	1.11
	Average	15.46		1.26(2.6)		15.61		1.66(2.5)		15.44		1.72(2.4)	
Mean Value of Both Evaluations			1.30(3.4)				1.71(3.2)				1.77(3.1)		

a) The statistical uncertainties in % as obtained from the fits are given in brackets.

b)  $\chi$  is the square root of  $\chi^2$  divided by the number of datapoints minus the number of free parameters, the so called error adjustment factor of the fits.

Table VI Results for the Capture Width of the Unresolved Multiplet Composed by the s-Wave Resonance at 12.5 keV and the p-Waves at 12.2 and 13.6 keV in  $^{60}\text{Ni}$  not yet Corrected for Detector Efficiency <sup>a)</sup>

Run	Graphite Converter				Bismuth Graphite Converter				Bismuth Converter				
	$E_n$ (keV)	$\Gamma_n$ (keV)	$\Gamma_\gamma$ (eV)	$\chi^b$	$E_n$ (keV)	$\Gamma_n$ (keV)	$\Gamma_\gamma$ (eV)	$\chi^b$	$E_n$ (keV)	$\Gamma_n$ (keV)	$\Gamma_\gamma$ (eV)	$\chi^b$	
Evaluation 1: $\Gamma_n$ Free Parameter Average	I	12.65	1.98(9.7)	3.10(11.1)	1.01	12.74	1.88(11.1)	3.83(12.5)	1.02	12.62	2.18(9.1)	3.91(10.1)	0.94
	II	12.60	2.20(10.0)	3.20(10.3)	0.93	12.67	2.24(11.5)	3.87(13.0)	0.86	12.57	2.20(9.5)	4.06(9.6)	1.02
	III	12.46	1.89(10.7)	3.24(11.1)	1.02	12.56	2.10(15.3)	3.77(16.3)	1.21	12.49	1.92(11.7)	3.86(12.1)	1.02
	IV	12.47	1.95(7.1)	3.08(7.6)	0.87	12.55	1.99(13.0)	3.43(15.6)	1.14	12.38	1.94(11.7)	3.63(12.0)	1.26
	Average	12.55	2.01	3.15(5.0)		12.63	2.05	3.72(7.2)		12.51	2.06	3.86(5.5)	
Evaluation 2: $\Gamma_n$ Fixed Parameter Average	I	12.50	2.66	3.09(13.0)	1.09	12.62	2.66	3.78(15.6)	1.09	12.54	2.66	3.91(11.0)	0.98
	II	12.46		3.29(12.6)	1.17	12.40		3.87(15.8)	1.25	12.41		3.88(14.3)	1.13
	III	12.56		3.27(10.2)	0.97	12.64		3.96(12.6)	0.88	12.57		4.18(9.8)	1.06
	IV	12.27		3.08(11.2)	1.10	12.27		3.59(15.9)	1.10	12.21		3.75(14.5)	1.33
	Average	12.45		3.18(5.9)		12.48		3.80(7.5)		12.43		3.93(6.2)	
Mean Value of Both Evaluation			3.17(5.5)				3.76(7.4)				3.90(5.9)		

a) and b) same as in Table V

Table VII Results for the s-Wave Resonance at 27.7 keV in  $^{56}\text{Fe}$   
not yet Corrected for Detector Efficiency <sup>a)</sup>.

Sample Thickness (mm)	Graphite Converter				Bismuth Graphite Converter				Bismuth Converter			
	$E_n$ (keV)	$\Gamma_n$ (keV)	$\Gamma_\gamma$ (eV)	$\chi^b$	$E_n$ (keV)	$\Gamma_n$ (keV)	$\Gamma_\gamma$ (eV)	$\chi^b$	$E_n$ (keV)	$\Gamma_n$ (keV)	$\Gamma_\gamma$ (eV)	$\chi^b$
Evaluation 1:												
$\Gamma_n$ Free 0.3	27.85	2.06(10.5)	1.05(4.8)	0.95	27.90	1.47(14.5)	1.17(5.1)	0.94	27.71	1.34(12.7)	1.13(4.8)	0.89
Parameter 2.0	27.94	2.01(12.4)	1.05(6.1)	1.21	27.94	1.85(13.6)	1.17(6.0)	1.03	27.85	1.90(11.6)	1.15(5.9)	1.04
Average	27.84	2.03	1.05(3.9)		27.92	1.66	1.17(3.9)		27.78	1.62	1.14(3.8)	
Evaluation 2:												
$\Gamma_n$ Fixed 0.3	27.89	1.4	0.97(3.7)	1.05	27.88	1.4	1.17(3.7)	0.95	27.71	1.4	1.15(5.0)	0.92
Parameter 2.0	27.98		1.07(5.1)	1.30	27.97		1.18(4.9)	1.05	27.85		1.16(5.2)	1.15
Average	27.94		1.02(3.1)		27.94		1.18(3.0)		27.78		1.16(3.6)	
Mean Value Both Evaluation			1.03(3.5)				1.17(3.5)				1.15(3.7)	

a) and b) same as in Table V

Table VIII Results for Unresolved Multiplets of p-Wave Resonances  
in  $^{58}\text{Ni}$ , not yet Corrected for Detector Efficiency

Resonance Energies (keV)	Run	Graphite Converter	Bismuth-Graphite Converter	Bismuth Converter
		$g\Gamma_{\gamma} \Gamma_n / \Gamma$ (eV)	$g\Gamma_{\gamma} \Gamma_n / \Gamma$ (eV)	$g\Gamma_{\gamma} \Gamma_n / \Gamma$ (eV)
Evaluation 1 13.4 13.6	I	1.09	1.13	1.29
	II	1.16	1.26	1.37
	III	1.26	1.46	1.34
	IV	1.05	1.29	1.19
	average	1.14	1.29	1.30
Evaluation 2 13.4 13.6	I	1.31	1.32	1.39
	II	1.24	1.37	1.48
	III	1.26	1.57	1.39
	IV	1.16	1.35	1.29
	average	1.24	1.40	1.39
19.0 20.0 21.1	I	1.11	1.30	1.23
	II	1.15	1.31	1.19
	III	1.06	1.21	1.36
	IV	1.05	1.24	1.25
	average	1.09	1.26	1.26
26.1 26.6	I	1.26	1.62	1.50
	II	1.29	1.53	1.45
	III	1.24	1.54	1.55
	IV	1.27	1.50	1.46
	average	1.27	1.55	1.49

Table IX Results for Unresolved Multiplets of p-Wave Resonances  
in  $^{60}\text{Ni}$  not yet Corrected for Detector Efficiency

Resonance Energies (keV)	Run	Graphite Converter	Bismuth-Graphite Converter	Bismuth-Converter
		$g_{\gamma}^{\Gamma} \Gamma_n^{\Gamma} / \Gamma$ (eV)	$g_{\gamma}^{\Gamma} \Gamma_n^{\Gamma} / \Gamma$ (eV)	$g_{\gamma}^{\Gamma} \Gamma_n^{\Gamma} / \Gamma$ (eV)
23.8 <sup>a</sup>	I	0.76	0.75	0.81
	II	0.74	0.79	0.77
23.9	III	0.71	0.92	0.76
	IV	0.68	0.77	0.75
	average	0.72	0.81	0.77
28.5	I	1.74	1.99	1.81
28.6 (s-wave)	II	1.74	1.89	1.87
29.5	III	1.91	1.95	1.90
30.2	IV	1.77	1.84	1.88
33.0				
	average	1.79	1.92	1.87

a) these two resonances were fitted as a single resonance

Table X Results for Unresolved Multiplets of p-Wave Resonances  
in  $^{56}\text{Fe}$  not yet Corrected for Detector Efficiency

Resonance Energies (keV)	Sample Thickness (mm)	Graphite Converter	Bismuth-Graphite Converter	Bismuth Converter
		$g_{\gamma}^{\Gamma} \Gamma_n / \Gamma$ (eV)	$g_{\gamma}^{\Gamma} \Gamma_n / \Gamma$ (eV)	$g_{\gamma}^{\Gamma} \Gamma_n / \Gamma$ (eV)
22.7	0.3	0.18	0.25	0.21
	2.0	0.19	0.22	0.23
	average	0.18	0.24	0.22
<hr/>				
34.2	0.3	1.15	1.34	1.32
36.7	2.0	1.13	1.34	1.33
38.3	average	1.14	1.34	1.33

Table XI Results for p-Wave Resonances in  $^{58,60}\text{Ni}$  and  $^{56}\text{Fe}$  after Correction for Detector Efficiency

Isotope	Resonance Energies (keV)	Graphite Converter	Bismuth-Graphite Converter	Bismuth-Converter	Average
		$g \Gamma_n \Gamma_\gamma / \Gamma$ (eV)			
$^{58}\text{Ni}$	13.4, 13.6	1.22	1.31	1.24	1.26
	19.0, 20.0, 21.1	1.12	1.22	1.17	1.17
	26.1, 26.6	1.30	1.51	1.38	1.40
$^{60}\text{Ni}$	23.8, 23.9	0.72	0.79	0.73	0.75
	28.5, 28.6, 29.5	1.80	1.88	1.77	1.82
	30.2, 33.0				
$^{56}\text{Fe}$	22.7	0.18	0.24	0.21	0.21
	34.2, 36.7, 38.3	1.15	1.32	1.27	1.25
corrected Results form Ref. 1					
	22.7	0.16			0.16
	34.2, 36.7, 38.3	1.17			1.17

Table XII Final Results for the s-Wave Resonances in  $^{58,60}\text{Ni}$  and  $^{56}\text{Fe}$

Isotope	Resonance Energy (keV)	Graphite Converter	Bismuth-Graphite Converter	Bismuth Converter	Average	Uncertainty (%)		
		$\Gamma_{\gamma}$ (eV)	$\Gamma_{\gamma}$ (eV)	$\Gamma_{\gamma}$ (eV)	$\Gamma_{\gamma}$ (eV)	statistical	systematic	total
$^{58}\text{Ni}$	15.35	1.41	1.63	1.56	1.53	1.9	6.3	6.6
$^{60}\text{Ni}^a$	12.5	2.88	3.07	2.88	2.92	3.5	5.6	6.6
$^{56}\text{Fe}$	27.7	1.07	1.14	1.06	1.09	2.1	4.6	5.1
corrected result from Ref. 1:								
$^{56}\text{Fe}$	27.7	1.05			1.05	1.3	4.7	4.9
averaged value from Ref. 1 and present work								
$^{56}\text{Fe}$	27.7				1.06	1.1	4.7	4.8

a) a value  $g\Gamma_{\gamma}\Gamma_n/\Gamma = 0.56$  eV has been subtracted from the fitted resonance area to account for the unresolved p-wave resonances at 12.2 and 13.6 keV

Table XIII Systematic Uncertainties of the Capture Width of s-Wave Resonances in  $^{58,60}\text{Ni}$  and  $^{56}\text{Fe}$  as Evaluated for the Data Measured with the Graphite Converter <sup>a</sup>.

	$^{58}\text{Ni}(15.35 \text{ keV})$				$^{60}\text{Ni}(12.5 \text{ keV})$				$^{56}\text{Fe}(27.7 \text{ keV})$		
	Run	I	II	III	IV	I	II	III	IV	V(0.3 mm)	V(2.0 mm)
Measured Sample											
Flight Path transformation		0.8	0.8	0.8	0.8	0.8	0.8	0.8	0.8	0.8	0.8
Constant background		1.2	1.7	1.3	1.4	1.6	2.4	2.1	1.9	1.8	0.6
Gold Sample:											
Flight Path transformation		0.7	0.7	0.7	0.7	0.7	0.7	0.7	0.7	0.7	0.7
Constant background		0.7	0.7	0.5	0.8	0.8	0.8	0.6	1.0	0.1	0.3
Multiple scattering		0.7	0.7	0.7	0.7	0.7	0.7	0.7	0.7	0.7	0.7
Capture cross section		2.5	2.5	2.5	2.5	2.5	2.5	2.5	2.5	2.5	2.5
Neutron beam intensity		0.4	0.4	0.6	0.4	0.4	0.4	0.6	0.4	0.5	1.0
Gamma-ray self absorption		1.0	1.0	1.0	1.0	1.0	1.0	1.0	1.0	1.0	1.0
FANAC calculation		2.0	2.0	2.0	2.0	2.0	2.0	2.0	2.0	2.0	2.0
Energy scale		1.0	1.0	1.0	1.0	1.0	1.0	1.0	1.0	1.0	1.0
Subtraction of p-waves		3.0	3.0	3.0	3.0	2.0	2.0	2.0	2.0	-	-
Detector efficiency		3.7	3.7	3.7	3.7	2.9	2.9	2.9	2.9	2.2	2.2
Total systematic uncertainty		6.2	6.3	6.2	6.3	5.4	5.7	5.6	5.6	4.7	4.5
Averaged value of all runs			6.3				5.6				4.6

a) all values are given in %

Table XIV Contribution of the Investigated s-Wave Resonances  
to Fast Reactor Averaged Neutron Capture Cross Sections

Resonance	Relative Contribution to Total Capture Rate of the Respective Isotope (%)		Relative Contribution to Total Capture Rate of All Structural Materials (%)	
	$\Gamma_{\gamma}$ taken from Ref. 15	$\Gamma_{\gamma}$ from present results	$\Gamma_{\gamma}$ taken from Ref. 15	$\Gamma_{\gamma}$ from present results
$^{56}\text{Fe}$ (27.7 keV)	11	8	5.1	3.7
$^{58}\text{Ni}$ (15.4 keV)	20	16	2.0	1.6
$^{60}\text{Ni}$ (12.5 keV)	46	37	1.8	1.4

Table XV Maxwellian Average Cross Sections for Various Thermal Energies

Thermal Energy (keV)	$\langle\sigma v\rangle$ (mb)			
	$^{58}\text{Ni}$		$^{60}\text{Ni}$	
	total	contribution of s-wave resonance at 15.4 keV a)	total	contribution of s-wave resonance at 12.5 keV a)
20	45.7	13.7 (30.0 %)	40.9	21.6 (52.8 %)
25	41.8	11.1 (26.6 %)	35.2	16.3 (46.3 %)
30	39.0 $\pm$ 2.5	9.5 (24.4 %)	31.4 $\pm$ 1.6	12.8 (40.8 %)
35	36.9	8.3 (22.5 %)	28.7	10.5 (36.6 %)
40	35.4	7.5 (21.2 %)	26.8	8.8 (32.8 %)

a) The relative amount of the total cross section in % is given in brackets

Table XVI Summary of Adopted Parameters for the Calculation of Level Densities and Radiative Widths

Model parameter	Adopted values		
	$^{58}\text{Ni}$	$^{60}\text{Ni}$	$^{56}\text{Fe}$
$a$ ( $\text{MeV}^{-1}$ )	7.32	8.4	8.52
$U_x$ (MeV)	8.2	7.25	6.9
$T$ (MeV)	1.31	1.16	1.14
$\beta$	.17	.17	-.25
$\sigma^2$	7.3	4.5	5.1
$D_{\text{OBS}}$ (keV)	14.	14.	19.
$E_1$ (MeV)	16.0	16.0	17.5
$\Gamma_1$ (MeV)	3.7	3.7	4.8
$\sigma_1$ (mb)	53	55	77
$E_2$ (MeV)	18.6	18.4	21.4
$\Gamma_2$ (MeV)	5.1	5.1	4.95
$\sigma_2$ (mb)	75	78	39
$E_R$ (MeV)	11.8	11.7	12.0
$\Gamma_R$ (MeV)	2.36	2.34	2.4
$\sigma_R$ (mb)	10.6	11.0	10.3

Table XVII Level Schemes Adopted for the Compound Nuclei  
 $^{59}\text{Ni}$ ,  $^{61}\text{Ni}$  and  $^{57}\text{Fe}$  a)

Level Number	Energy (MeV)	Spin	Parity	Branching Ratio (level number, probability %)				
$^{59}\text{Ni}$								
1	0.	1.5	-	-				
2	0.339	2.5	-	(1,100)				
3	0.465	.5	-	(1,100)				
4	0.878	1.5	-	(1,99)	(1,1)			
5	1.190	2.5	-	(1,92)	(2,8)			
6	1.302	.5	-	(1,75)	(3,12)	(4,13)		
7	1.338	3.5	-	(2,100)				
8	1.685	2.5	-	(1,14)	(2,84)	(3,2)		
9	1.735	1.5	-	(1,61)	(2,17)	(3,11)	(5,11)	
10	1.739	4.5	-	(2,100)				
11	1.746	(1.5)	(-)	(1,100)				
12	1.768	4.5	-	(2,50)	(7,50)			
13	1.778	(1.5)	(-)	(1,100)				
14	1.948	3.5	-	(2,86)	(5,9)	(7,5)		
15	2.33	2.5	-	(1,5)	(2,32)	(4,12)	(5,6)	
16	2.349	5.5	-	(1,54)	(12,46)			
17	2.415	1.5	-	(1,38)	(2,26)	(3,21)	(4,10)	(5,5)
18	2.428							
19	2.533							
20	2.536	6.5						
21	2.629	3.5	-					
22	2.682							
23	2.691							
24	2.705	5.5	-					
25	2.713	1.5	-					
$^{61}\text{Ni}$								
1	0.	1.5	-					
2	0.067	2.5	-	(1,100)				
3	0.283	.5	-	(1,100)				
4	0.655	1.5	-	(1,74)	(2,9)	(3,17)		
5	0.959	2.5	-	(1,80)	(2,18)	(3,2)		
6	1.015	3.5	-	(1,100)				
7	1.1	1.5	-	(1,40)	(2,9)	(3,51)		
8	1.132	2.5	-	(1,62)	(2,38)			
9	1.186	1.5	-	(1,88)	(2,2)	(3,2)	(4,8)	
10	1.457	3.5	-	(1,57)	(2,43)			
11	1.611	2.5	-	(1,45)	(2,55)			
12	1.73	1.5	-	(1,44)	(2,35)	(3,17)	(4,4)	
13	1.812	2.5	(-)	(2,100)				
14	1.978							
15	1.99							
16	1.996	1.5	-					
17	2.02	3.5	-					
18	2.123	4.5	+					
19	2.124	0.5	-					

Table XVII cont'd

Level Number	Energy (MeV)	Spin	Parity	Branching Ratio (level number, probability %)				
$^{57}\text{Fe}$								
1	0.	.5	-					
2	.014	1.5	-	(1,100)				
3	.136	2.5	-	(1,11)	(2,89)			
4	.367	1.5	-	(1,15)	(2,77)	(3,8)		
5	.706	2.5	-	(1,4)	(2,86)	(3,8)	(4,2)	
6	1.007	3.5	-	(2,36)	(3,64)			
7	1.198	4.5	-	(3,100)				
8	1.265	.5	-	(2,80)	(4,20)			
9	1.357	3.5	-	(5,100)				
10	1.628	1.5	-	(2,64)	(4,28)	(5,8)		
11	1.726	1.5	-	(1,79)	(5,21)			
12	1.975	(0.5)	(-)	(1,35)	(2,32)	(3,22)	(4,11)	
13	1.989	4.5	-	(3,84)	(5,13)	(6,3)		
14	2.117	2.5	-	(1,32)	(2,30)	(3,22)	(4,12)	(5,4)
15	2.207	2.5	-	(1,33)	(2,29)	(3,22)	(4,12)	(5,4)
16	2.219	(1.5)	(-)	(1,28)	(2,27)	(3,22)	(4,15)	(5,8)
17	2.335	1.5	-	(1,30)	(2,30)	(3,22)	(4,13)	(5,5)
18	2.355	5.3	-	(6,59)	(7,28)	(9,13)		
19	2.454	.5	+	(1,100)				
20	2.455	(4.5)	(+)	(6,100)				
21	2.506	2.5	+	(4,100)				
22	2.565	(1.5)	(-)	(1,30)	(2,29)	(3,22)	(4,13)	(5,6)
23	2.597	(1.5)	(-)	(1,30)	(2,29)	(3,22)	(4,13)	(5,6)
24	2.697	.5	-	(1,30)	(2,28)	(3,22)	(4,14)	(5,6)
25	2.763							
26	2.818							
27	2.829							
28	2.835	(.5)	(-)					
29	2.855							
30	2.879	6.5	-					
31	2.9	(.5)	(-)					

a) The experimental information is taken from Refs. (43,44).  
 The  $J, \pi$  characteristics within parenthesis are arbitrarily assigned.  
 Underlined gamma decay probabilities have been assigned according to Weisskopf estimates for M1 transitions assuming that single particle state transitions dominate.

Table XVIII      Calculated Average E1 and M1 Contributions  
to the Total Radiative Width for s-, p- and  
d-Wave Resonances Compared to Results Evaluated  
from Experimental Data

Isotope	l	$J^\pi$	$\bar{\Gamma}_\gamma$ (E1)	$\nu_{\text{eff}}$	$\bar{\Gamma}_\gamma$ (M1)	$\nu_{\text{eff}}$	$\bar{\Gamma}_\gamma^{\text{EXP}}$	$\nu_{\text{eff}}^{\text{EXP}}$
$^{58}\text{Ni}$	0	$1/2^+$	2200 $\pm$ 883	12	113 $\pm$ 38	17		
	1	$1/2^-$	766 $\pm$ 244	20	456 $\pm$ 234	8		
		$3/2^-$	726 $\pm$ 230	20	380 $\pm$ 153	12		
	2	$3/2^+$	1823 $\pm$ 602	18	106 $\pm$ 36	18		
		$5/2^+$	1387 $\pm$ 444	20	97 $\pm$ 32	18		
$^{60}\text{Ni}$	0	$1/2^+$	1050 $\pm$ 420	12	59 $\pm$ 21	16	1300 $\pm$ 70 <sup>a</sup>	
	1	$1/2^-$	443 $\pm$ 148	18	208 $\pm$ 98	9	1200 <sup>a</sup>	
		$3/2^-$	401 $\pm$ 132	19	190 $\pm$ 69	15		
	2	$3/2^+$	1109 $\pm$ 353	20	53 $\pm$ 18	17		
		$5/2^+$	896 $\pm$ 268	22	45 $\pm$ 15	18		
$^{56}\text{Fe}$	0	$1/2^+$	1070 $\pm$ 428	11	34 $\pm$ 12	15		850 $\pm$ 410 <sup>b</sup>
	1	$1/2^-$	246 $\pm$ 87	16	203 $\pm$ 97	9	500 $\pm$ 180 <sup>b</sup>	17.1
		$3/2^-$	231 $\pm$ 75	19	162 $\pm$ 64	13		
	2	$3/2^+$	900 $\pm$ 313	17	32 $\pm$ 11	18		
		$5/2^+$	652 $\pm$ 224	17	25 $\pm$ 8	18		

<sup>a</sup> from Ref. 2

<sup>b</sup> from Ref. 27

Table XIX Calculated Partial and Total Gamma Widths and Cross Sections for s-Wave Resonances. Quoted Uncertainties are the Standard Deviation of the Corresponding Distributions

$E_\lambda$ (keV)	$E_{\text{LEVEL}}$ (keV)	$\Gamma_\lambda^{\circ}$ (eV)	$\Gamma_\gamma^{\text{STAT}}$ (meV)	$\sigma^{\text{STAT}}$ (mb)	$\Gamma_\gamma^{\text{VAL}}$ (meV)	$\sigma^{\text{TOT}}_1$ (mb)	$\Gamma_\gamma^{\text{TOT}}$ (meV)	$\sigma^{\text{TOT}}_2$ (mb)	$\Gamma_\gamma^{\text{EXP}}$ (meV)
$^{58}\text{Ni}$									
15.4		9.19	2200 $\pm$ 40%	141 $\pm$ 40%	62	145	1745 $\pm$ 50%	112 $\pm$ 50%	1530 $\pm$ 7%
	0		340	13.7	35	15.1	150	6.3	124 $\pm$ 17 <sup>a</sup>
	465		305	10.1	18	10.7	176	5.8	110 $\pm$ 19 <sup>a</sup>
	878		237	8.0	3	8.9	188	6.4	
	1302		183	6.0	6	6.2	121	4.0	
	1735		139	4.6	0	4.6	126	0.0	
$^{60}\text{Ni}$									
12.3		23.98	1050 $\pm$ 40%	42 $\pm$ 40%	127	5	1670 $\pm$ 50%	66 $\pm$ 50%	2920 $\pm$ 7%
	0		178	3.4	60	4.5	444	8.4	514 $\pm$ 72 <sup>a</sup>
	283		150	2.8	57	3.8	380	7.2	289 $\pm$ 46 <sup>a</sup>
	656		117	2.2	1	2.2	142	2.7	
	1100		87	1.6	3	1.7	123	2.3	
	1186		82	1.5	6	1.6	132	2.5	
$^{56}\text{Fe}$									
27.7		8.72	1070 $\pm$ 40%	33 $\pm$ 40%	145	37.8 $\pm$ 40%	650 $\pm$ 50%	21.3 $\pm$ 50%	1090 $\pm$ 5%
	0		183	2.37	12	2.52	103	1.33	145 $\pm$ 25 <sup>a</sup>
	14		182	3.04	71	4.22	26	.43	35 $\pm$ 13 <sup>a</sup>
	367		146	2.44	39	3.09	34	.57	
	1265		80	1.01	18	1.232	23	.29	
	1628		61	1.01	2	1.045	40	.66	
	1726		57	0.95	3	1.007	32	.67	

a) Ref. (45)

Table XX Capture Cross Section of  $^{58,60}\text{Ni}$  and  $^{56}\text{Fe}$  in  
Dependence of the Multiplicity of the Capture Cascade a)

Multiplicity	Total Capture	s-wave		p-wave		d-wave	
		$1/2^+$	$1/2^-$	$3/2^-$	$3/2^+$	$5/2^+$	
$^{58}\text{Ni}$							
$\sigma$	100	49	12	36	1	2	
1	10	17.5	3.5	2.	11	11.5	
2	43.5	55.5	32	31.	57	41	
3	35.5	24.5	48.5	46.5	28	38	
4	9.5	2.5	14	18.	4	8.5	
5	1.5	-	2	2.5	-	1	
$\langle m \rangle$	2.5	2.12	2.81	2.9	2.25	2.5	
$^{60}\text{Ni}$							
$\sigma$	100	43	13	41	1	2	
1	9	17	3	2	11	9.5	
2	35.5	45.5	28	27.5	48.5	43	
3	40.5	32	47.5	47.5	34.5	40.5	
4	13.5	5.5	19	20	6	7	
5	1.5	-	2.5	3	-	-	
$\langle m \rangle$	2.63	2.26	2.9	2.95	2.35	2.45	
$^{56}\text{Fe}$							
$\sigma$	100	35	10	33	6	16	
1	8	16	4	3	11	0	
2	27	32	31	21	26	24	
3	33.5	32	31	32	41.5	41.5	
4	25.5	17	26	33	18.5	29	
5	5.5	1.5	7	10	3	5.5	
6	0.5	-	1	1	-	-	
$\langle m \rangle$	2.95	2.55	3.0	3.3	2.76	3.16	

a)

All values, except for the average multiplicity  $\langle m \rangle$  are given in %  
the calculations have been performed at the neutron energy of the s-wave resonances.

FIGURE CAPTIONS

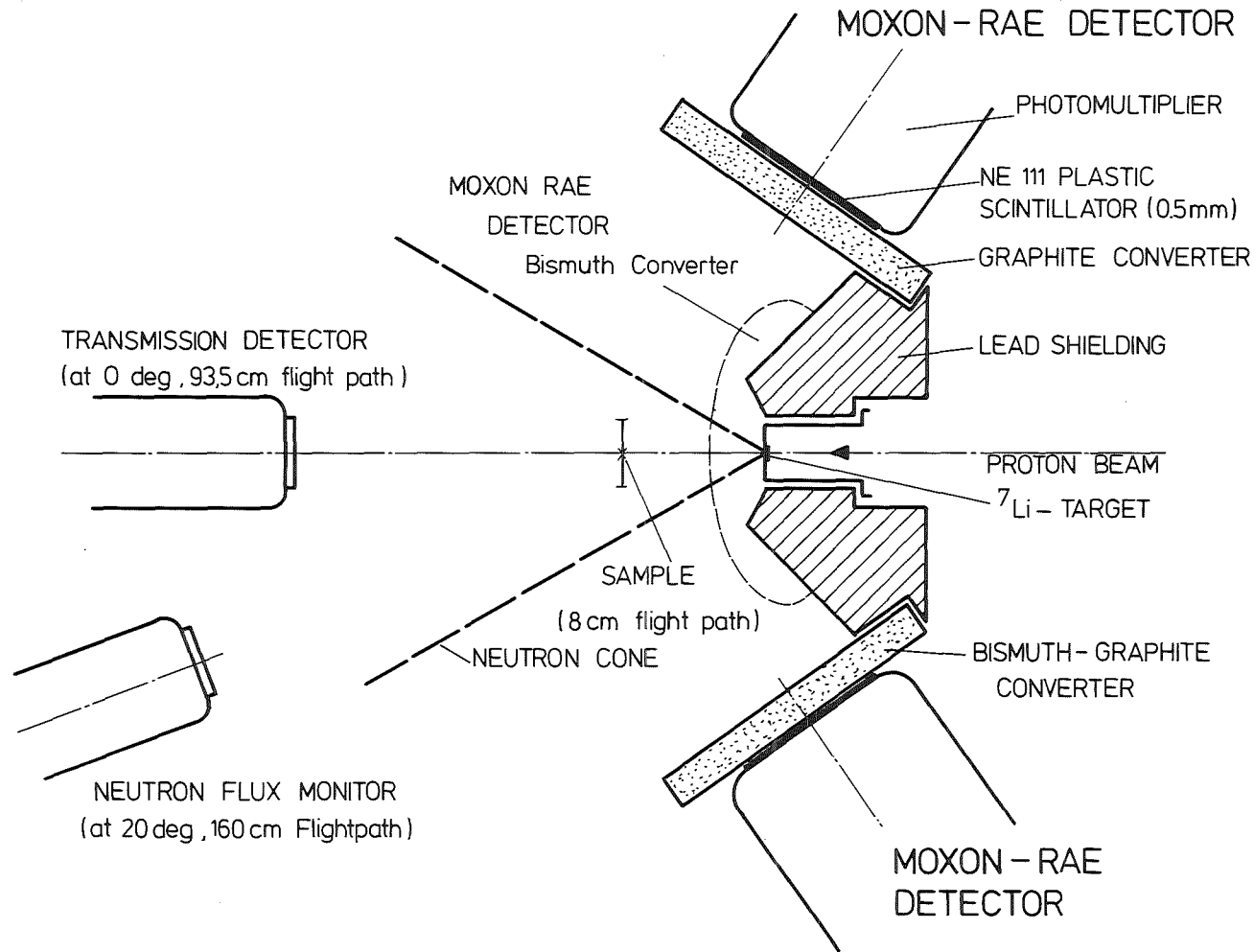
- Fig. 1 Schematic view of the experimental setup.
- Fig. 2 TOF spectra of  $^{58,60}\text{Ni}$  samples and the corresponding background as measured with three Moxon Rae detectors with graphite, bismuth-graphite and bismuth converters, respectively (Run II, sample thickness 0.3 mm, flight path 87.8 mm).
- Fig. 3 TOF spectra of  $^{58,60}\text{Ni}$  samples and the corresponding background as measured with the graphite converter in Runs I, III and IV.
- Fig. 4 TOF spectra of  $^{56}\text{Fe}$  samples and the corresponding background as measured with the graphite converter in Run V.
- Fig. 5 Fanac fits to the capture yield of  $^{58}\text{Ni}$  as evaluated from the TOF spectra shown in Fig. 2.
- Fig. 6 Fanac Fits to the capture yield of  $^{60}\text{Ni}$  as evaluated from the TOF spectra shown in Fig. 2.
- Fig. 7 Fanac fits to the capture yield of  $^{58}\text{Ni}$  as evaluated from the TOF spectra shown in Fig. 3.
- Fig. 8 Fanac fits to the capture yield of  $^{60}\text{Ni}$  as evaluated from the TOF spectra shown in Fig. 3.
- Fig. 9 Fanac fits to the capture yield of  $^{56}\text{Fe}$  as evaluated from the TOF spectra shown in Fig. 4.
- Fig. 10 The shape of the detector efficiency for Moxon Rae detectors with different converter materials.

Fig. 11 Comparison between the calculated cumulative number of levels (solid line) and known discrete levels for all compound nuclei. The energy  $E_{\text{cut}}$  where the level continuum was supposed to start is marked by an arrow. In the respective inserts, the theoretical spin distribution (dashed line) and the spin distribution of discrete levels below  $E_{\text{cut}}$  are given.

Fig. 12 Calculated capture gamma-ray spectra for s-wave resonances in  $^{58,60}\text{Ni}$  and  $^{56}\text{Fe}$ .  
The results obtained from the statistical model, statistical model and valence capture, as well as considering the interference term are given separately.

Fig. 13 Calculated capture gamma-ray spectra for p- and d-wave resonances in  $^{58,60}\text{Ni}$  and  $^{56}\text{Fe}$ .

Fig. 1



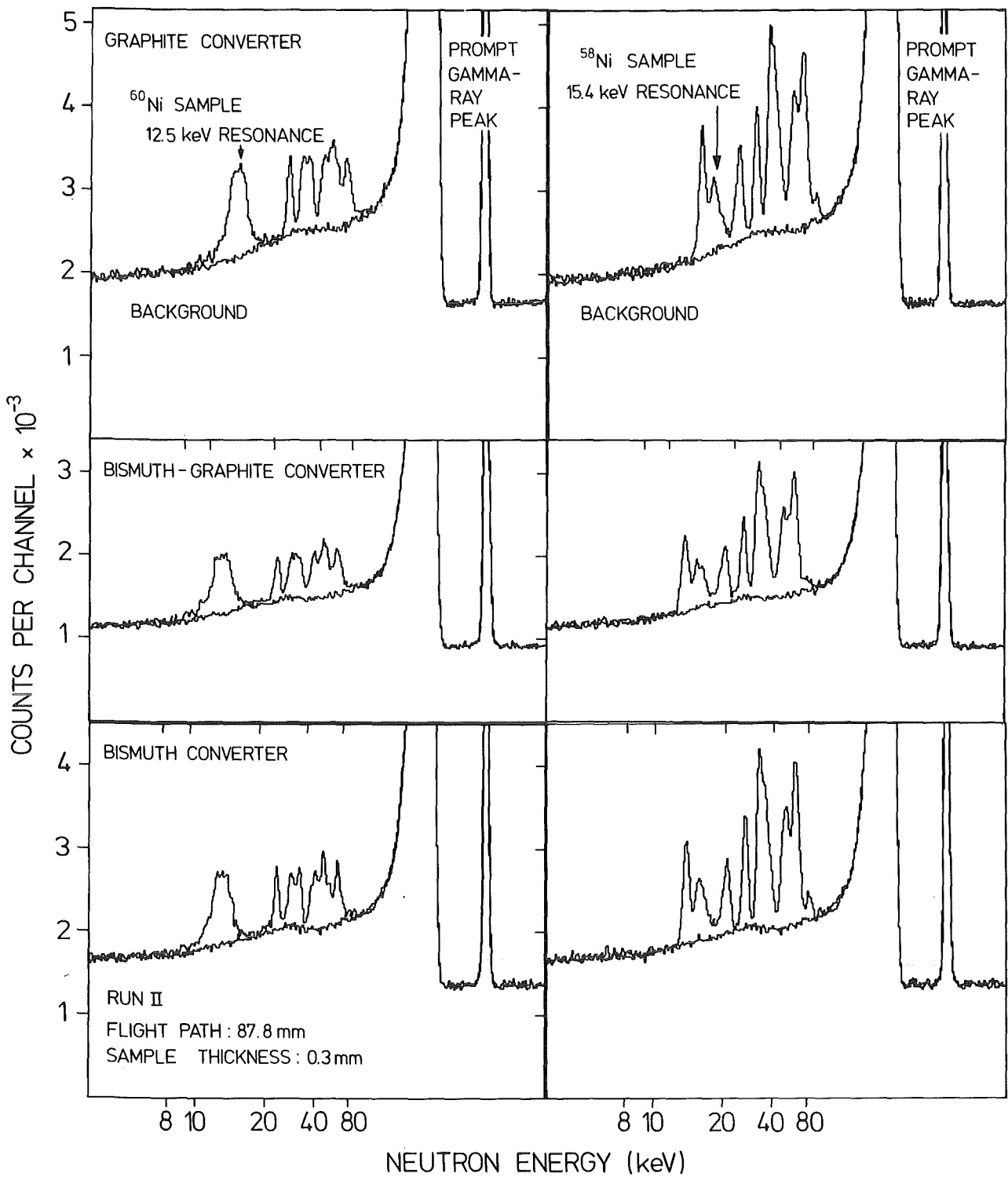


Fig. 2

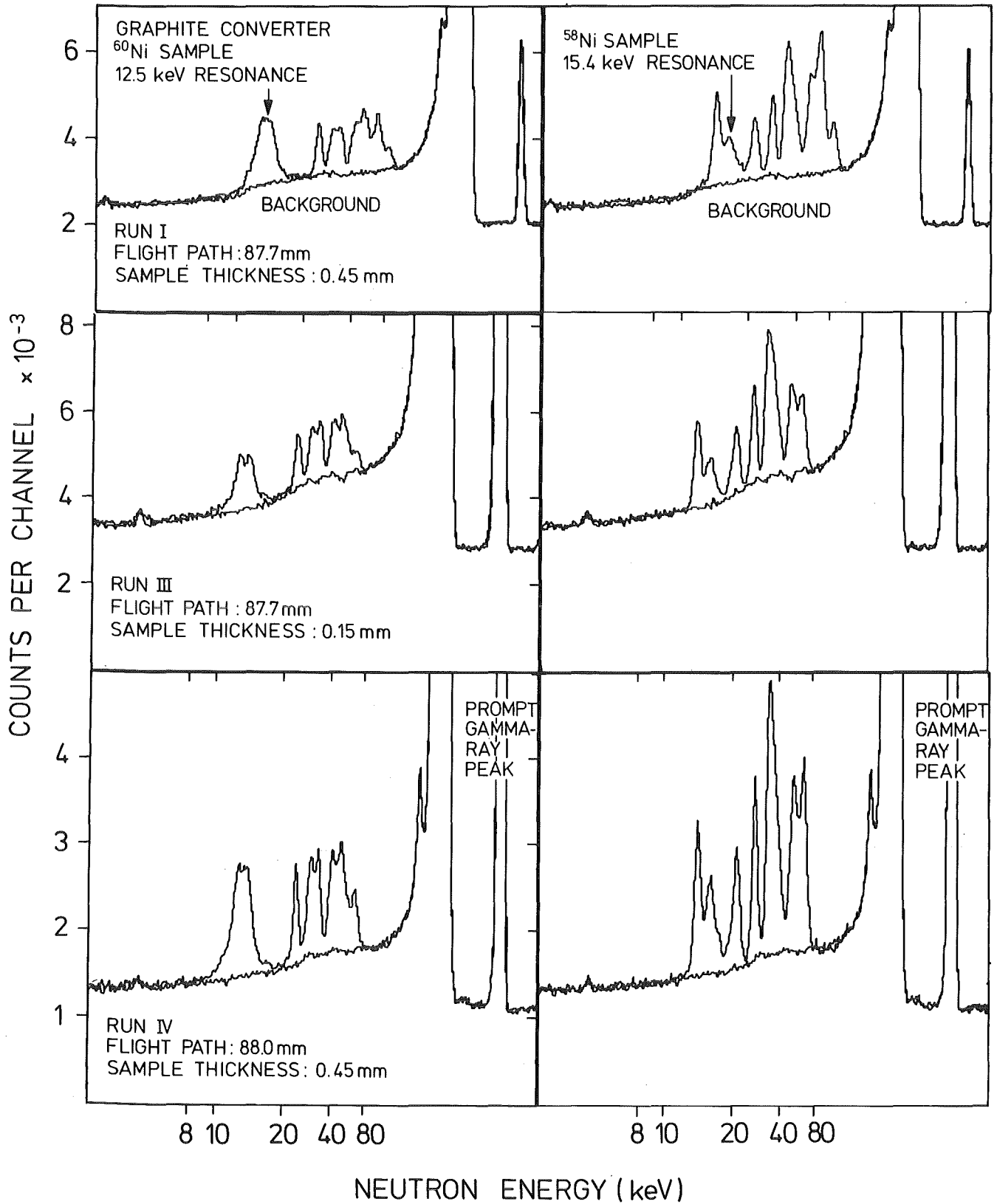
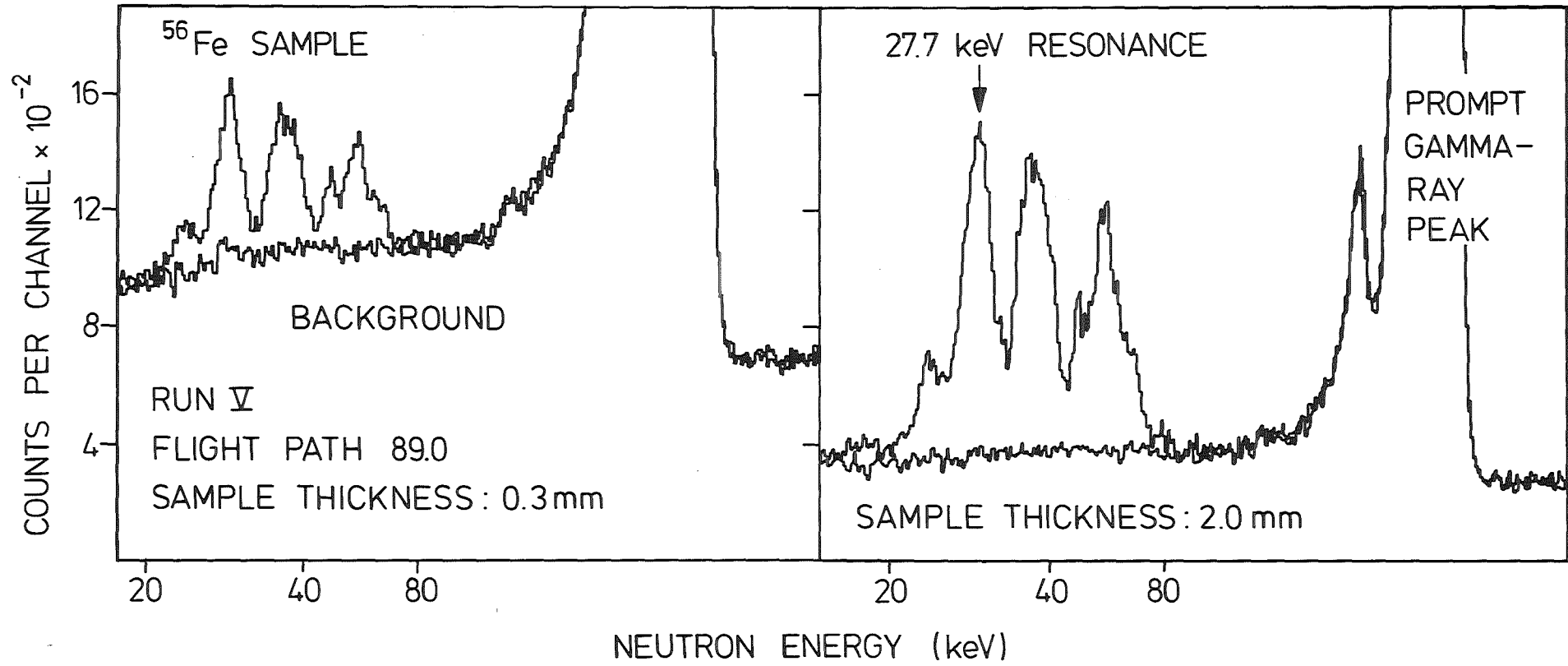


Fig. 3

Fig. 4



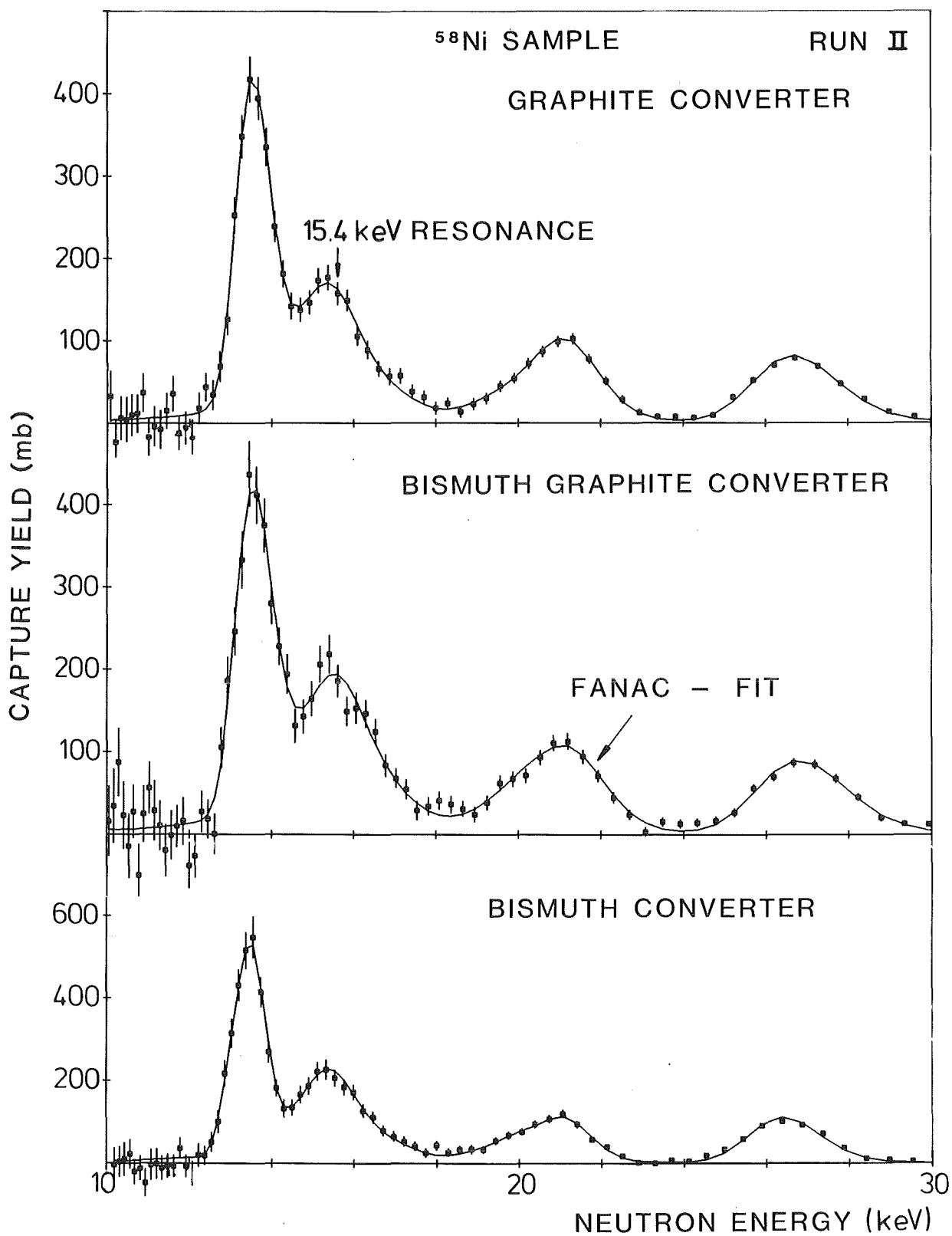


Fig. 5

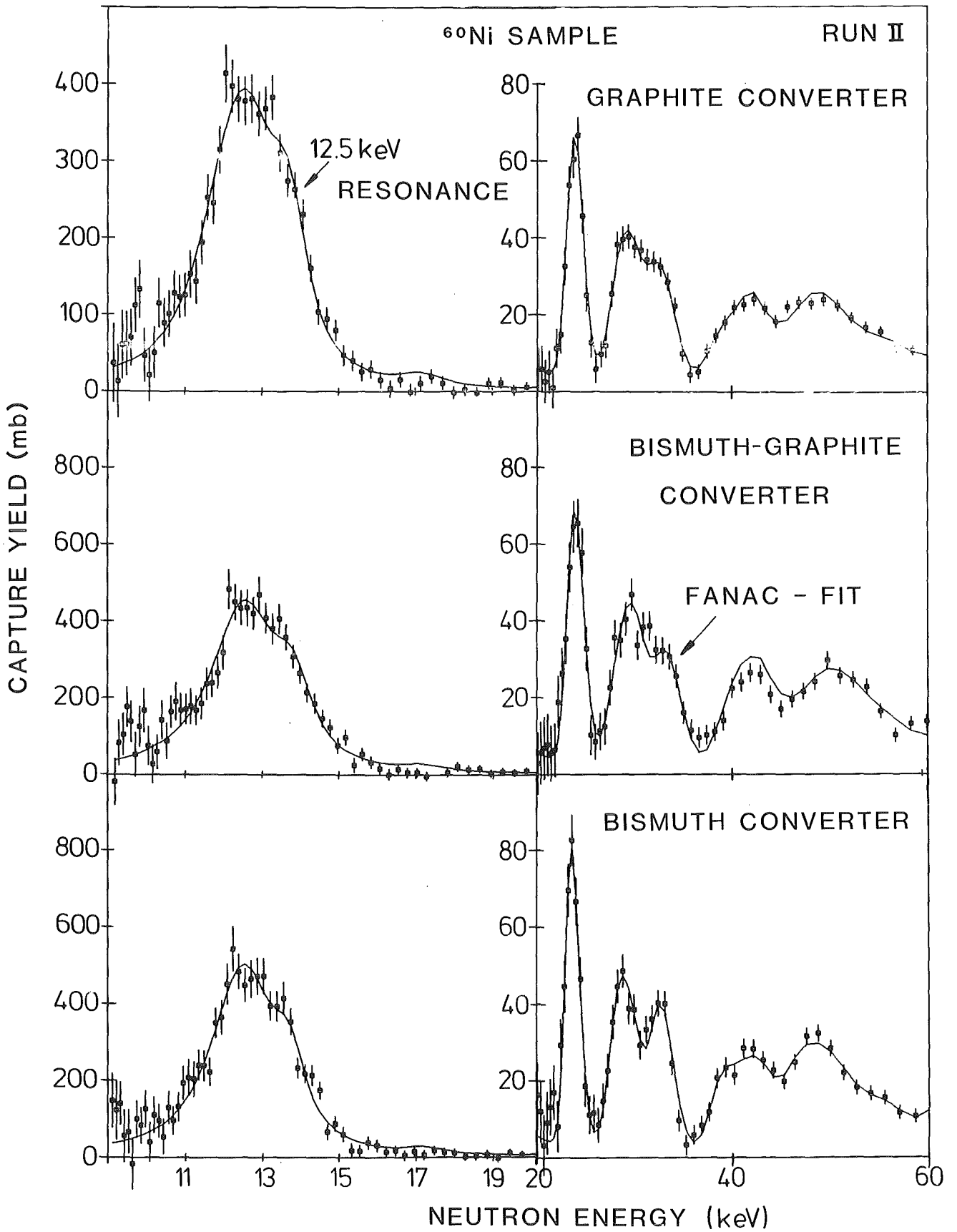


Fig. 6

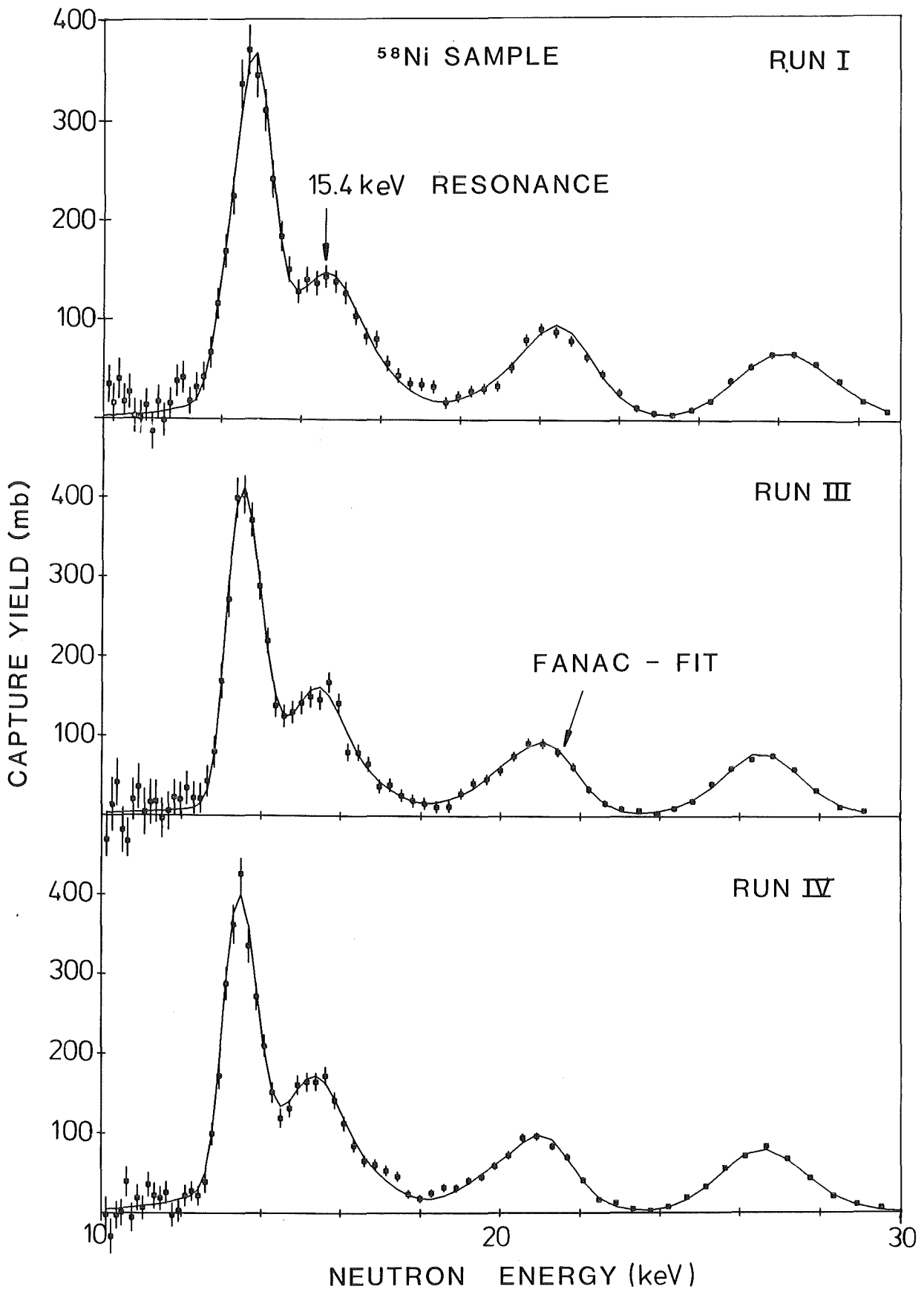


Fig. 7

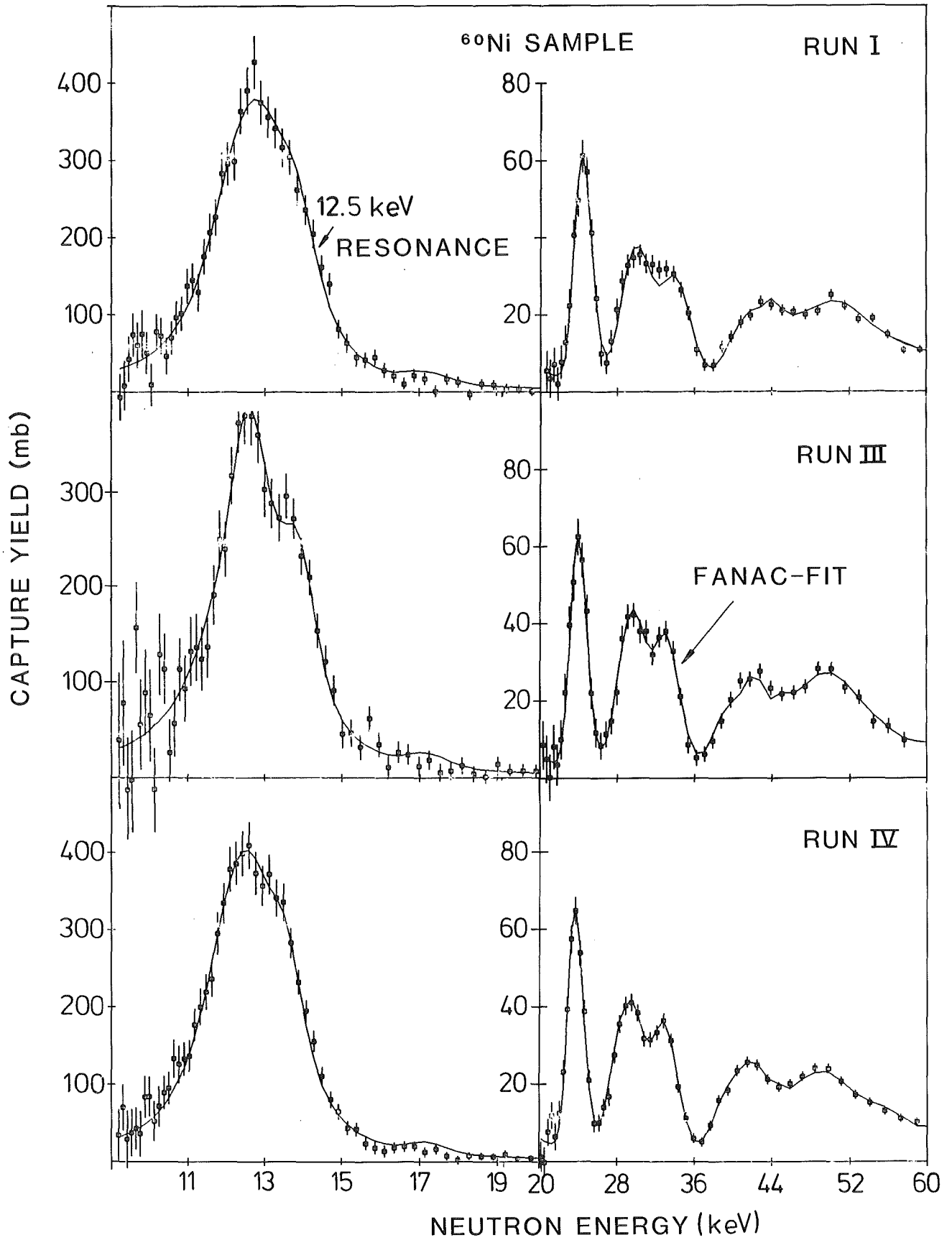
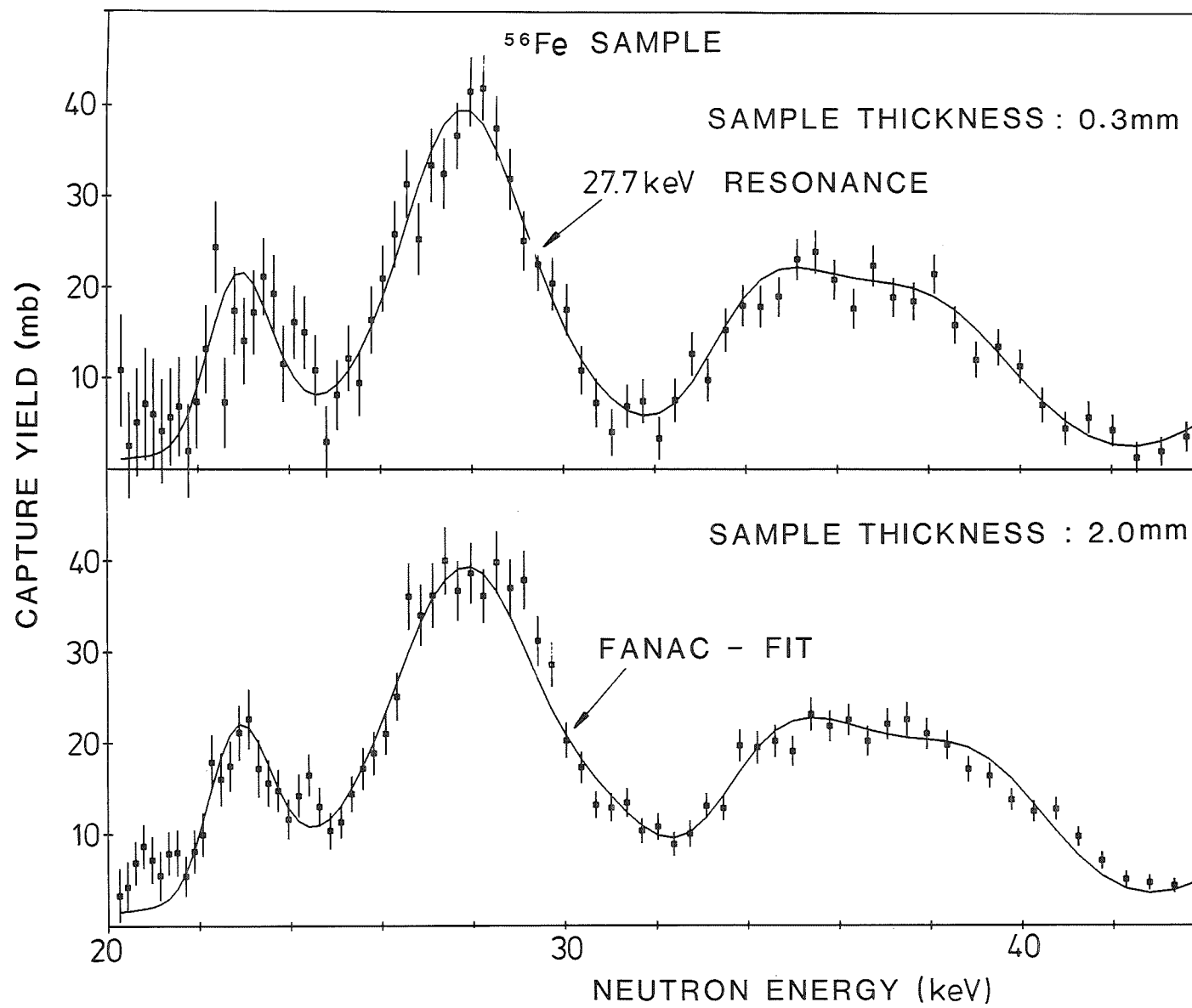


Fig. 8

Fig. 9



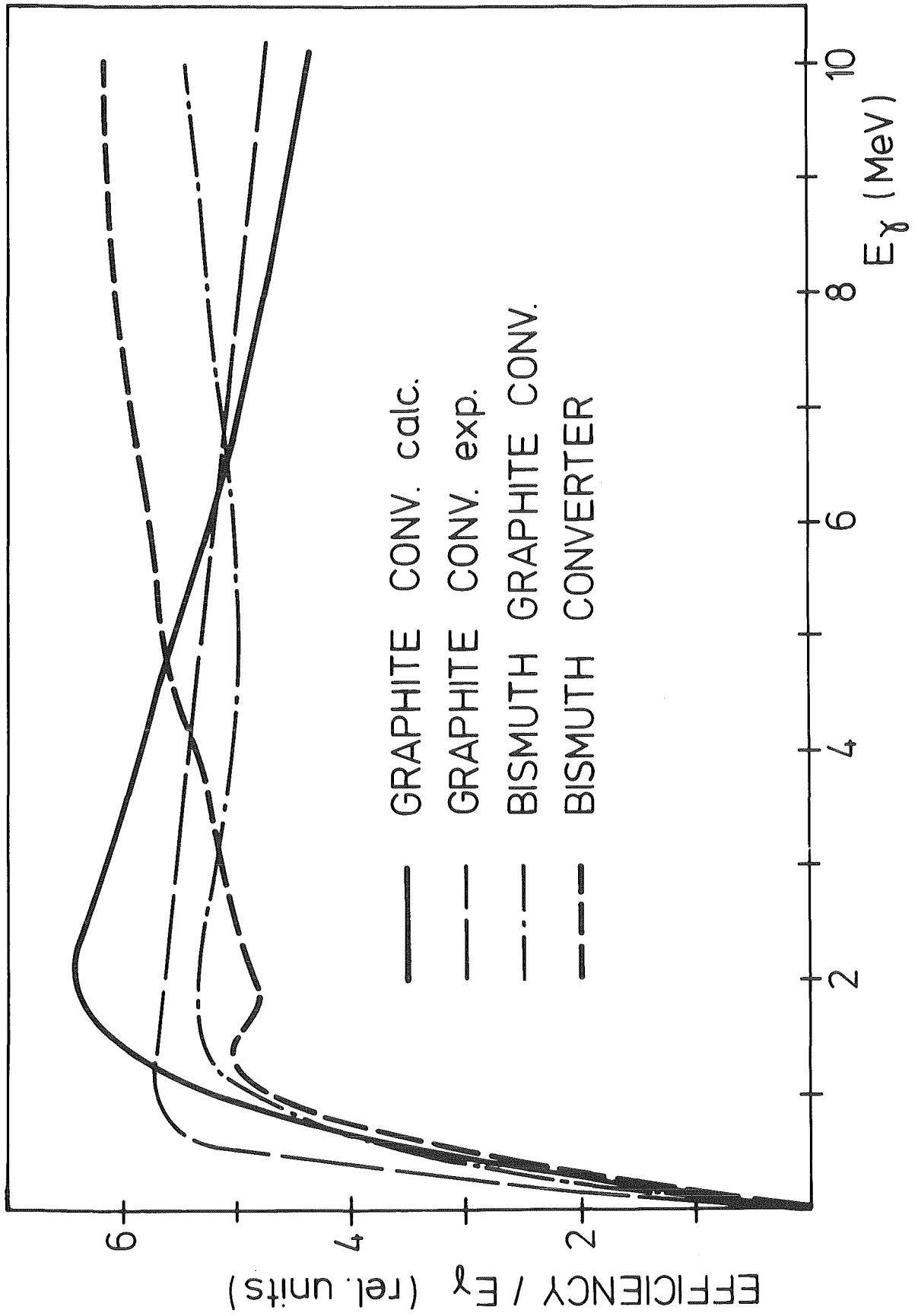


Fig. 10

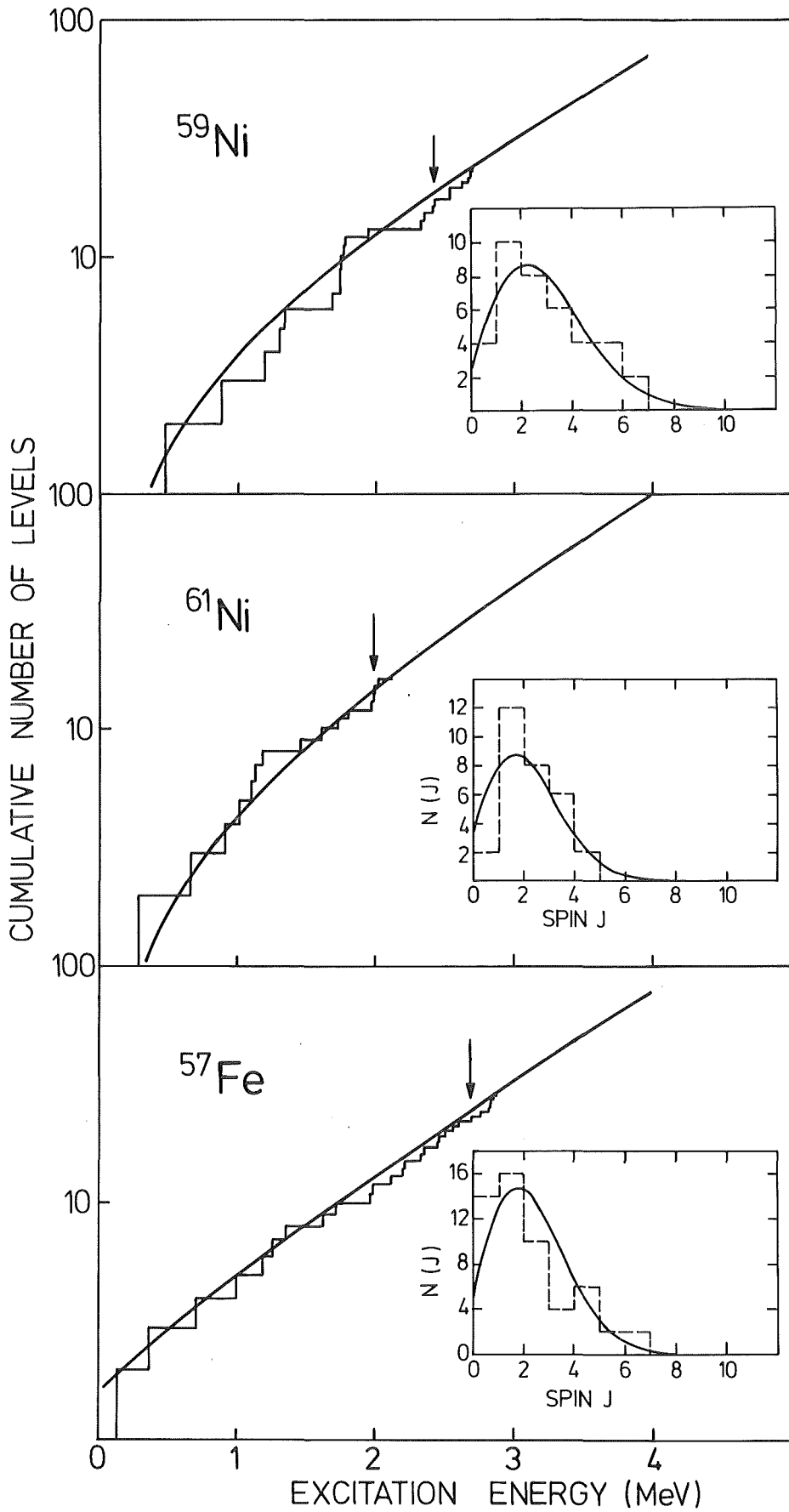


Fig. 11

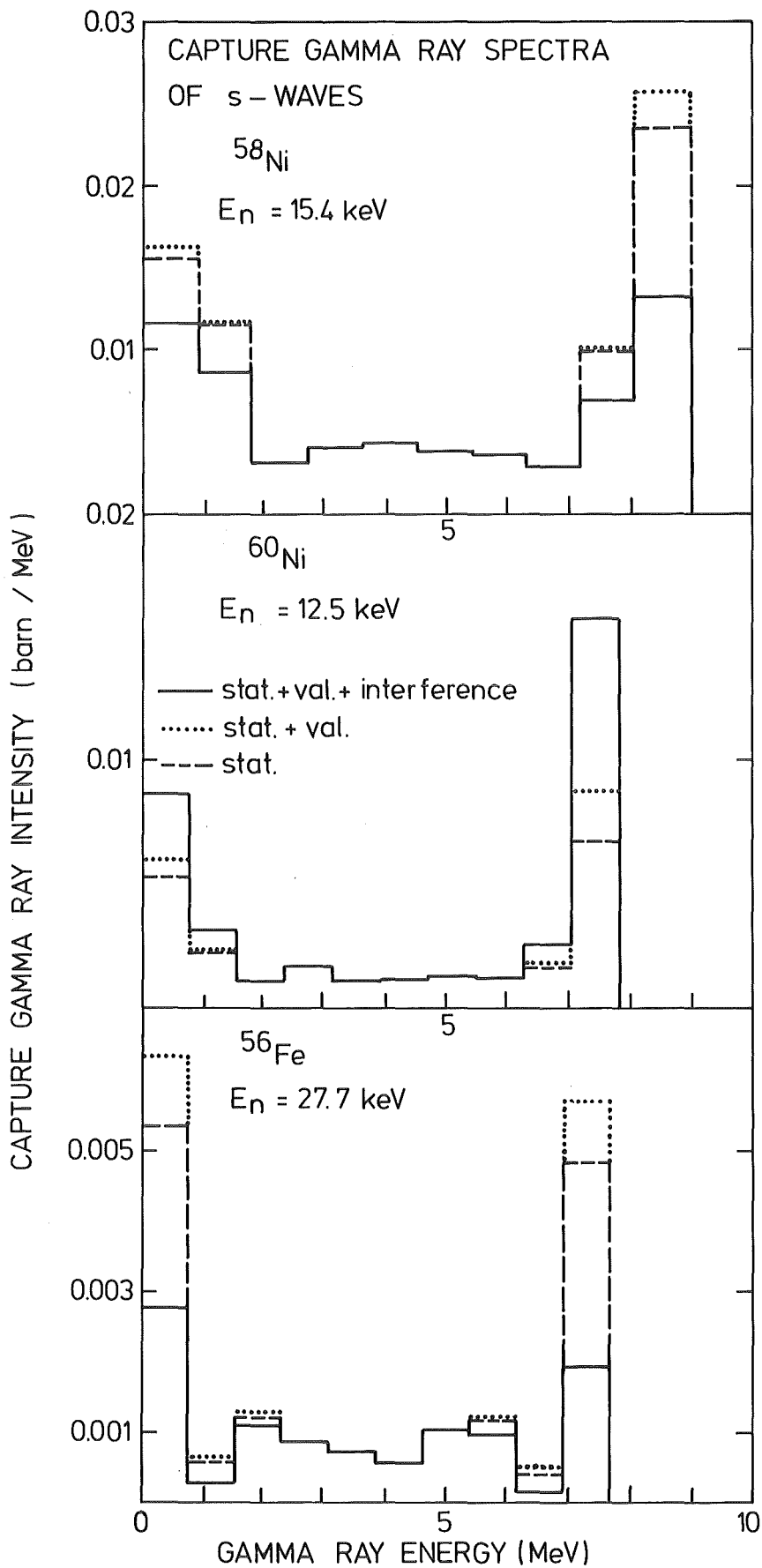


Fig. 12

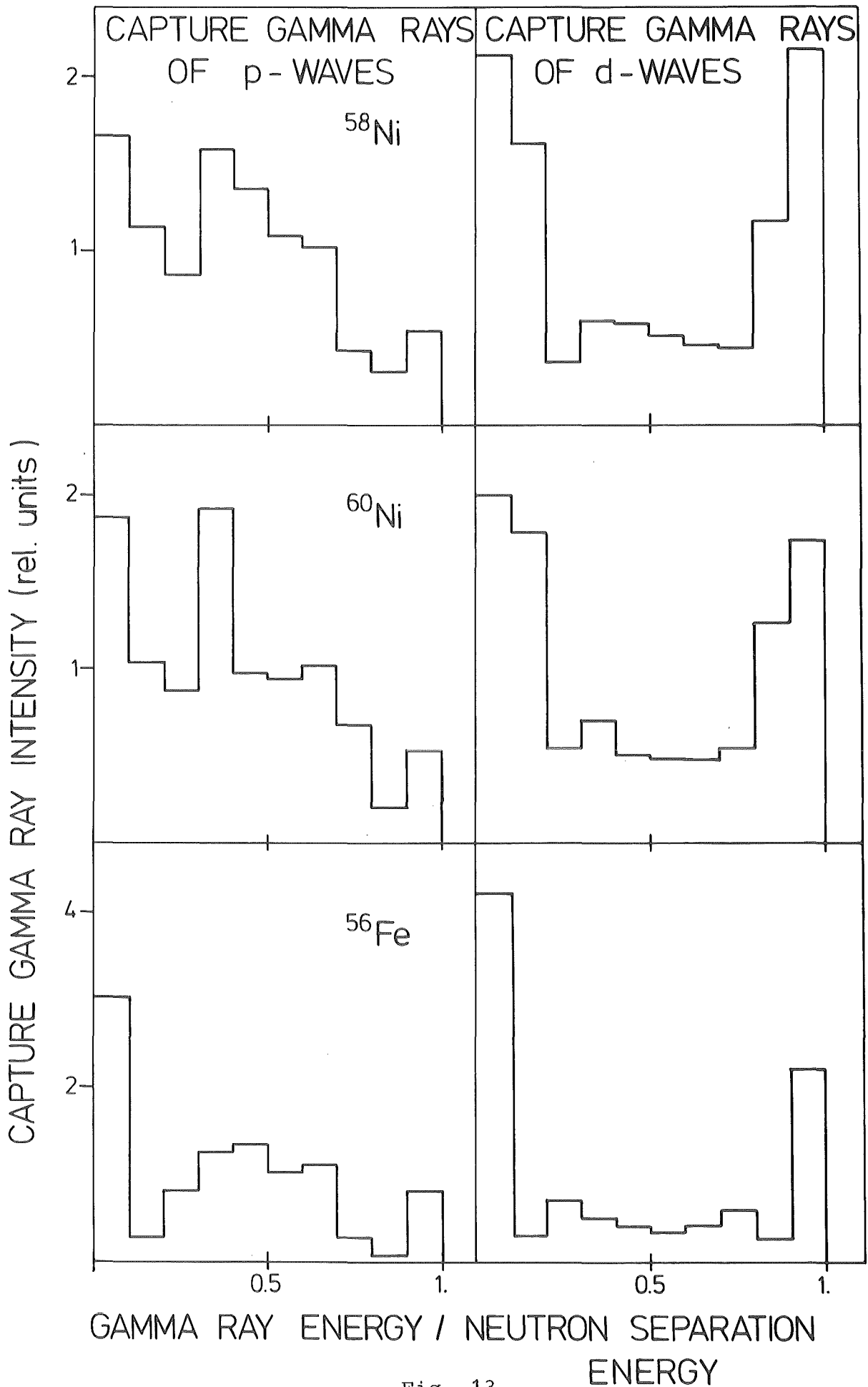


Fig. 13